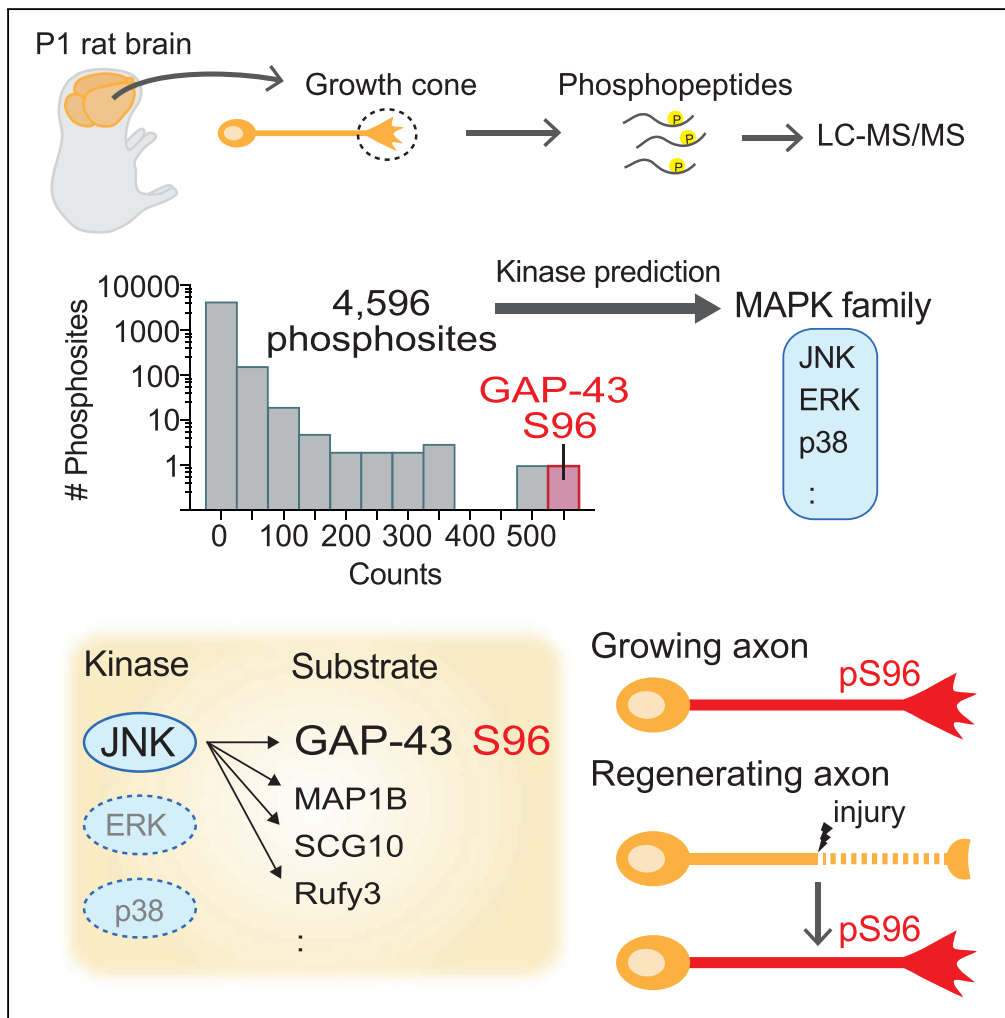


Article

# Growth Cone Phosphoproteomics Reveals that GAP-43 Phosphorylated by JNK Is a Marker of Axon Growth and Regeneration



Asami Kawasaki,  
Masayasu Okada,  
Atsushi  
Tamada, ...,  
Yukihiko Fujii,  
Kosei Takeuchi,  
Michihiro Igarashi

tarokaja@med.niigata-u.ac.jp

**HIGHLIGHTS**

Phosphoproteomics of mammalian growth cone membranes reveals activation of MAPK

JNK is the activated MAPK in growth cones and phosphorylates S96 of GAP-43

pS96 of GAP-43, the most frequent site, is observed in growing axons

pS96 is biochemically detected in the regenerating axons of the peripheral nerves

Kawasaki et al., iScience 4, 190–203  
June 29, 2018 © 2018 The Authors.  
<https://doi.org/10.1016/j.isci.2018.05.019>



## Article

# Growth Cone Phosphoproteomics Reveals that GAP-43 Phosphorylated by JNK Is a Marker of Axon Growth and Regeneration

Asami Kawasaki,<sup>1,2,10</sup> Masayasu Okada,<sup>1,2,3,10</sup> Atsushi Tamada,<sup>1,2,4,10,11</sup> Shujiro Okuda,<sup>5</sup> Motohiro Nozumi,<sup>1,2</sup> Yasuyuki Ito,<sup>1</sup> Daiki Kobayashi,<sup>1</sup> Tokiwa Yamasaki,<sup>6,12</sup> Ryo Yokoyama,<sup>7</sup> Takeshi Shibata,<sup>7</sup> Hiroshi Nishina,<sup>6</sup> Yutaka Yoshida,<sup>8</sup> Yukihiro Fujii,<sup>3</sup> Kosei Takeuchi,<sup>1,2,9</sup> and Michihiro Igarashi<sup>1,2,13,\*</sup>

## SUMMARY

**Neuronal growth cones are essential for nerve growth and regeneration, as well as for the formation and rearrangement of the neural network. To elucidate phosphorylation-dependent signaling pathways and establish useful molecular markers for axon growth and regeneration, we performed a phosphoproteomics study of mammalian growth cones, which identified >30,000 phosphopeptides of ~1,200 proteins. The phosphorylation sites were highly proline directed and primarily MAPK dependent, owing to the activation of JNK, suggesting that proteins that undergo proline-directed phosphorylation mediate nerve growth in the mammalian brain. Bioinformatics analysis revealed that phosphoproteins were enriched in microtubules and the cortical cytoskeleton. The most frequently phosphorylated site was S96 of GAP-43 (growth-associated protein 43-kDa), a vertebrate-specific protein involved in axon growth. This previously uncharacterized phosphorylation site was JNK dependent. S96 phosphorylation was specifically detected in growing and regenerating axons as the most frequent target of JNK signaling; thus it represents a promising new molecular marker for mammalian axonal growth and regeneration.**

## INTRODUCTION

The growth cone, a specialized, highly motile structure formed at the tips of extending axons of developing neurons (Dent et al., 2011; Igarashi, 2014), is crucial for accurate synaptogenesis in the developing brain. In addition, growth cone activity is involved in the rearrangement of neuronal networks during neural plasticity and axonal regeneration in the adult brain (Bloom and Morgan, 2011; Gordon-Weeks and Fournier, 2014; Nozumi and Igarashi, 2017; Tamada and Igarashi, 2017). Therefore, to understand the mechanisms underlying neuronal network formation and maintenance, it is essential to elucidate the molecular pathways that determine growth cone behavior. At present, however, little molecular information is available regarding growth cones in the mammalian brain. Previously, we performed a proteomics analysis of mammalian growth cones and characterized approximately 1,000 unique proteins (Nozumi et al., 2009; see also Estrada-Bernal et al., 2012). The results of this analysis revealed novel molecular mechanisms underlying nerve growth (Igarashi, 2014; Nozumi et al., 2017; Honda et al., 2017a, 2017b).

To further investigate molecular signaling in growth cones, we focused on protein phosphorylation, the most important regulatory mechanism in many cellular processes (Humphrey et al., 2015a). To date, most efforts in this regard have used *in vitro* phosphorylation systems that do not necessarily represent the *in vivo* situation. Phosphoproteomics is an important, novel, and powerful technique for comprehensive and quantitative identification of *in vivo* phosphorylation sites (von Stechow et al., 2015) and should be able to establish novel molecular markers for axonal growth and regeneration.

Specifically, we performed phosphoproteomics analysis of the growth cone membrane (GCM; Ellis et al., 1985; Nozumi et al. 2009; Igarashi, 2014). From among more than 30,000 phosphopeptides, this analysis identified ~4,600 different phosphorylation sites from ~1,200 proteins. Surprisingly, proline (P)-directed phosphorylation was predominant, with more than 60% of serine (S) or threonine (T) phosphorylation sites predicted to depend on P-directed kinases. Bioinformatics analysis suggested that these frequent P-directed phosphorylation events were due to mitogen-activated protein kinase (MAPK) activation. In

<sup>1</sup>Department of Neurochemistry and Molecular Cell Biology, Graduate School of Medical and Dental Sciences, Niigata University, 1-757 Asahimachi, Chuo-ku, Niigata 951-8510, Japan

<sup>2</sup>Center for Trans-disciplinary Research, Institute for Research Promotion, Niigata University, Chuo-ku, Niigata 951-8510, Japan

<sup>3</sup>Department of Neurosurgery, Brain Research Institute, Niigata University, Chuo-ku, Niigata 951-8585, Japan

<sup>4</sup>Precursory Research for Embryonic Science and Technology, Japan Science and Technology Agency, Kawaguchi, Saitama 332-0012, Japan

<sup>5</sup>Laboratory of Bioinformatics, Graduate School of Medical and Dental Sciences, Niigata University, Chuo-ku, Niigata 951-8510, Japan

<sup>6</sup>Department of Developmental and Regenerative Biology, Medical Research Institute, Tokyo Medical and Dental University, Bunkyo-ku, Tokyo 113-8510, Japan

<sup>7</sup>K.K. Sciex Japan, Shinagawa-ku, Tokyo 140-0001, Japan

<sup>8</sup>Center for Coordination of Research, Institute for Research Promotion, Niigata University, Ikarashi, Niigata 951-2181, Japan

<sup>9</sup>Department of Medical Cell Biology, Aichi Medical University, Nagakute, Aichi 480-1195, Japan

<sup>10</sup>These authors contributed equally

Continued



particular, we found that c-Jun N-terminus kinase (JNK; Bogoyevitch et al., 2010) was the major active member of the MAPK family and was responsible for several heavily phosphorylated sites.

The most abundant phosphorylated site was S96 of neuronal growth-associated 43-kDa (GAP-43, also called as neuromodulin), a vertebrate neuron-specific protein involved in nerve growth (Skene, 1989; Denny, 2006; Holahan, 2017), comprising more than 1% of all phosphopeptides. This phosphorylated site was previously uncharacterized. Subsequent experiments revealed that S96 phosphorylation (pS96) was JNK dependent. A pS96 antibody (Ab) specifically recognized growing and regenerating axons, and pS96 was directly detected in regenerating axons by mass spectrometry (MS).

Taken together, our data show that JNK signaling is a key pathway for axon growth that is conserved across a wide range of animals. JNK signaling via vertebrate-specific substrates such as GAP-43 plays important roles in mammalian growth cones, and pS96 Ab represents a promising new molecular marker for mammalian axonal growth/regeneration.

## RESULTS

### High Frequency of P-Directed Phosphosites in GCMs

Phosphoproteomics analysis of GCM fractions isolated from postnatal day 1 (P1) rat forebrain identified more than 30,000 phosphopeptides at greater than 95% confidence (see Data S1). The condensation ratio of the phosphopeptides (i.e., the ratio of phosphopeptides to total peptides) was 95.9%. Thresholding with 1% false discovery rate (FDR) extracted 4,596 phosphorylation sites that corresponded to 1,223 proteins. Highly frequent phosphorylation sites are shown in Table S1.

We classified the kinase substrates in GCMs into various categories based on the number of phosphorylation sites (Figure 1A) and the frequency of phosphopeptides phosphorylated at S or T (Figure 1B). Cytoskeletal components and signaling proteins were the major GCM phosphoproteins identified in this manner (Figures 1A and 1B; see also Data S2, referring to the protein names). Among the phosphopeptides identified in GCMs, serine-proline (SP)/threonine-proline (TP) residues, i.e., P-directed-kinase-dependent phosphorylation sites (Villén et al., 2007; Huttlin et al., 2010), were highly enriched in the GCM (Figures 1B, 2A, and 2B; Table S1).

Protein kinases are classified into four major groups: acidic, basic, P directed, and others (Villén et al., 2007). P-directed sites constituted 63.9% of phosphoserine (pS) and 78.0% of phosphothreonine (pT) sites in all categories (Figure 1B; Data S1). The typical sequences of each protein kinase category were visualized using the IceLogo web server (Figure S1). The fraction of P-directed sites (Figures 2A and 2B) was higher than those estimated from a meta-analysis of two previous reports on phosphoproteomics (Lundby et al., 2013; Humphrey et al., 2015b; Figure S2).

Next, we predicted kinases that are responsible for the phosphorylation sites identified by our analysis. Using a kinase-specific phosphorylation site prediction tool KinasePhos (Huang et al., 2005; Wong et al., 2007), we found that MAPK is most likely to be a kinase responsible for the phosphorylation of SP/TP sites with high frequencies (Figure 2C). To elucidate the physiological functions of these substrates, we performed enrichment analysis using the GCM phosphorylation data, particularly for phosphopeptides that were phosphorylated  $\geq 20$  times (Figure 2B; Data S3). Two groups containing such highly phosphorylated sites, cytoskeleton-associated proteins (group I) and signaling proteins including cell adhesion molecules and guidance receptors (group II), were also highly enriched in the protein networks (Figure 2D). Substrates with P-directed phosphorylated sites (Figure 2C) were also enriched (Figure 2D). These proteins are thought to be involved in axon growth and guidance in mammalian brain (Dent et al., 2011; Igarashi, 2014; Short et al., 2016; Batty et al., 2017). Therefore, our results suggest that highly concentrated P-directed phosphoproteins in GCM play important functional roles in mammalian axon growth and guidance.

### P-Directed Phosphorylation of GCM Phosphoproteins Requires JNK Activity

The MAPK family includes extracellular-signal-regulated kinase (ERK), p38, and JNK, among which JNK appeared to be the most likely kinase candidate for mammalian GCM phosphorylation. First, several recent reports showed that JNK is involved in multiple steps of mammalian brain development (Oliva et al., 2006; Hirai et al., 2011; Barnat et al., 2010; Coffey, 2014). Second, JNK signaling is activated during axon

<sup>11</sup>Present address:  
Department of iPS Cell  
Applied Medicine, Kansai  
Medical University, Hirakata,  
Osaka 573-1010, Japan

<sup>12</sup>Present address:  
Department of Physiology,  
Keio University School of  
Medicine, Shinjuku-ku, Tokyo  
160-8582, Japan

<sup>13</sup>Lead Contact

\*Correspondence:  
tarokaja@med.niigata-u.ac.jp  
<https://doi.org/10.1016/j.isci.2018.05.019>

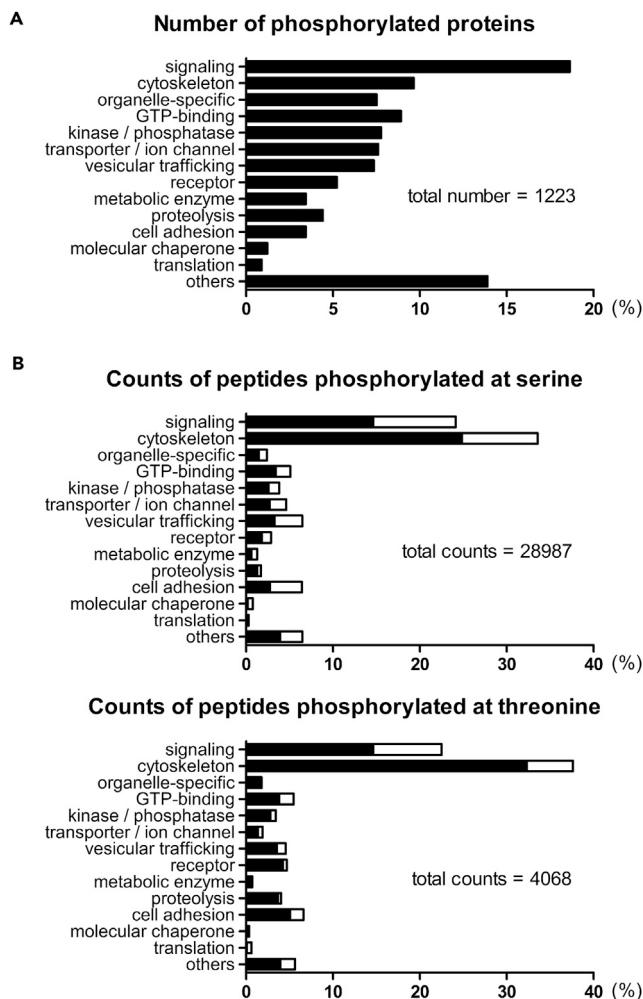


**Figure 1. GCM Phosphopeptides Derived from P1 Rat Brain Reveal a Large Number of P-Directed Kinase Substrates**

(A) Classification of phosphoproteins (1,223 proteins in total) that were derived from the phosphopeptides (4,596 species) detected by MS with 1% FDR. The value in each row represents the fraction of proteins in each functional category.

(B) Counts of peptides phosphorylated at serine (28,987 total counts) and threonine (4,068 total counts) that belong to each protein category. The counts were further divided into those for P-directed sites (filled bars) and those for non-P-directed sites (open bars).

regeneration, even in *C. elegans* (Nix et al., 2011). Together, these observations suggest the importance of JNK signaling in a wide range of organisms.

To test this hypothesis, we produced eight phospho-specific Abs against the high-frequency SP/TP phosphorylation sites (total number = 1,163, corresponding to 3.8% of the Conf95 phosphopeptides; Figure 3A; see also Tables S1 and S2). The most frequently phosphorylated site was S96 of GAP-43. When we chemically inhibited MAPK family members, only the JNK inhibitor SP600125 specifically blocked phosphorylation of GAP-43, as determined using phospho-specific Abs (Figures 3A and S3A; the antigen sequences are shown in Table S2). The intensities of two sites in GAP-43, S96 and T172, were decreased by SP600125 treatment (Figure 3B).

We also identified the upstream signal that activates JNK. In the brain, MKK7 is a specific activator of JNK (Yamasaki et al., 2011), and mice with brain-specific conditional knockout (cKO) of MKK7 exhibit hypoactive axon formation in the developing brain (Yamasaki et al., 2011, 2017). Using our phospho-specific Abs in this cKO mouse, we found that phosphorylation signals in the brain were greatly diminished, as also observed

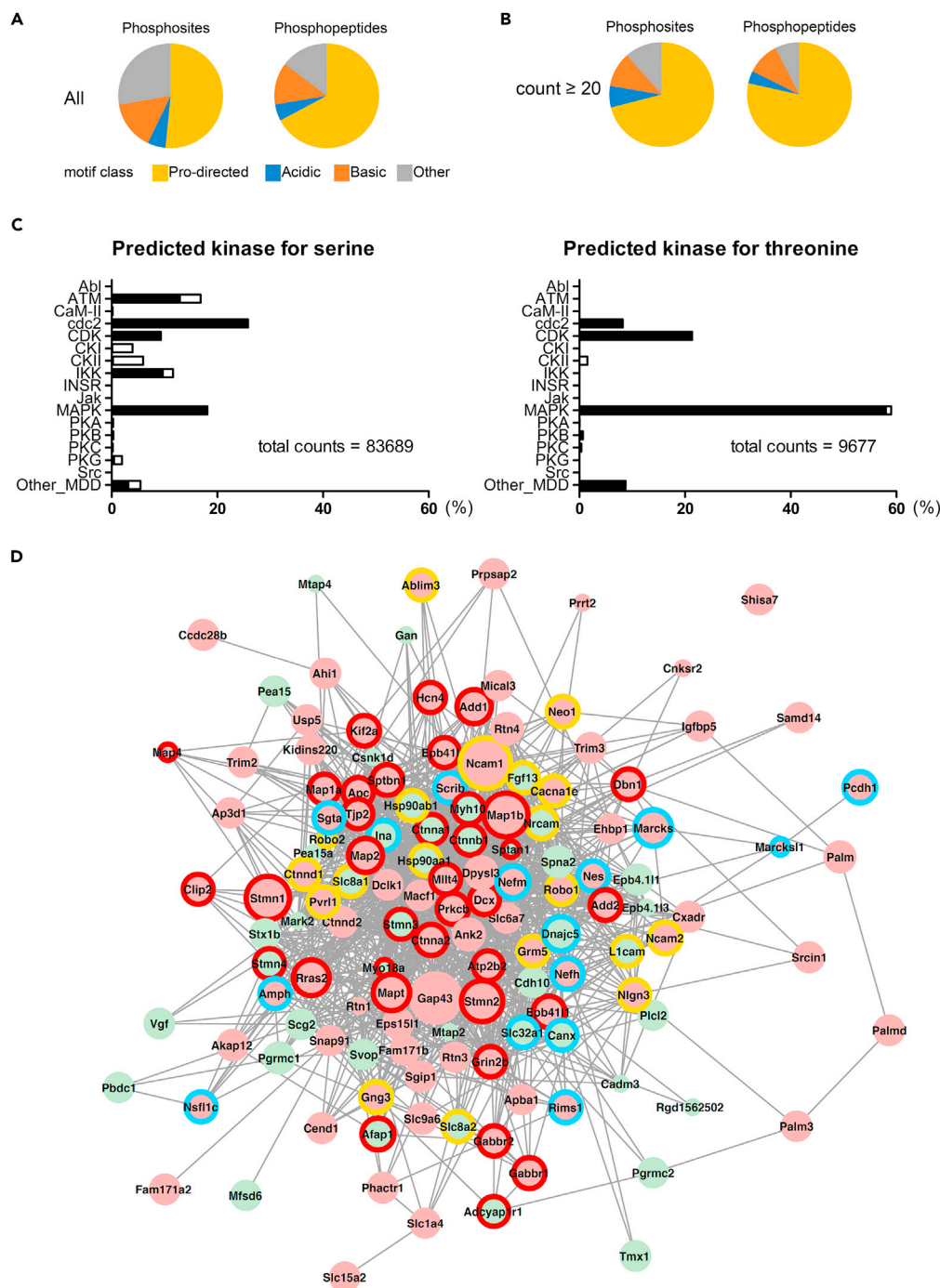


**Figure 2. Bioinformatics Analysis of Phosphosites Identified by GCM Phosphoproteomics of Rat P1 Brain Reveals that P-Directed Sites Are Mainly Dependent on MAPK**

(A and B) Fractions of phosphosites (*left*) and phosphopeptides (*right*) that are substrates of acid, basic, and proline-directed kinases for all data (A) or data thresholded by 20 counts (B).

(C) Protein kinases predicted for the serine (*left*) and threonine (*right*) phosphosites using KinasePhos server. The value in each row represents the fraction of phosphopeptides that are the targets of each kinase. The fractions were further divided into P-directed (*filled bars*) or non-P-directed (*open bars*) phosphorylation.

(D) Protein association network for P-directed and non-P-directed proteins. Protein association network was constructed using the STRING database (Szkarczyk et al., 2017), merged with data from human, rat, and mouse. Red and green filled circles indicate P-directed and non-P-directed phosphorylated proteins, respectively. The size of the circle for each

**Figure 2. Continued**

protein represents its phosphorylation frequency in GCM. The colors of the external rings indicate enriched protein network groups: group I (red), cytoskeletal proteins (microtubule-related proteins, cortical skeletal proteins, and actin-binding proteins); group II (yellow), signaling molecules related to axon growth/guidance (cell adhesion molecules, proteins in cAMP- or Ca<sup>2+</sup>-dependent signaling pathways, small GTPase signaling molecules, and guidance receptors); and group III (blue), other categories. Proteins without the external rings were not enriched.

with the chemical inhibitor (Figure 3C). By contrast, cyclin-dependent kinase 5 (CDK5) and glycogen synthase kinase 3 $\beta$  (GSK3 $\beta$ ) inhibitors did not prevent GAP-43 phosphorylation, suggesting that neither of these kinases is responsible for S96 or T172 phosphorylation (Figures S3B and S3C).

JNK has three isoforms: JNK1, JNK2, and JNK3 (Haeusgen et al., 2009; Coffey, 2014). Because JNK3 is not involved in early brain development (Kuan et al., 2003) and its expression is lower than that of the other two, we did not investigate its role in these experiments. Treatment of the cultured cortical neurons with small interfering RNAs (siRNAs) against JNK1 and JNK2 revealed that JNK1 plays a more important role in GAP-43 phosphorylation in mouse brain (Figures 3D and 3E), as expected (Hirai et al., 2011). JNK is activated in murine developing neurons (Chang et al., 2003). Taken together with our data, this observation suggests that JNK is responsible for the phosphorylation of many GCM proteins with SP/TP sites, such as S96 in GAP-43.

**Growing Axons Are Associated with pS96 GAP-43**

To further investigate the biological significance of the JNK-dependent, highly P-directed phosphosites in mammalian nerve growth, we focused on pS96 of GAP-43, both because it was the most abundant (Table S1) and because GAP-43 is a classical molecular marker for vertebrate axon growth and regeneration. pS96 Ab recognized exogenously expressed wild-type GAP-43 but not a mutant (S96A) lacking the phosphorylation site, especially under hyperosmotic conditions (0.5 M NaCl), which activate JNK (Figures S4A and S4B) (Zhang and Cohen, 1996).

In cultured mouse neurons, this pS96 Ab intensely labeled distal axons and growth cones with a punctate labeling pattern that was particularly concentrated at the growth cone (Figure 4A). Labeling was much weaker in proximal axons (Figure 4A) and other minor processes (Figure 4B). pS96 Ab immunoreactivity in growth cones was distributed along filopodial actin filaments and microtubules in the central domain (Figures 4C and 4D).

Immunohistochemical analyses revealed that pS96 Ab specifically recognized growing axons *in vivo* during development (Figures 5A–5C, S5A, and S5B). On embryonic day (E) 15, GAP-43 itself was expressed in most of the differentiated neurons, whereas by contrast, pS96 was localized to axonal processes but not present in cell bodies (Figure 5A). pJNK signals partially overlapped with those of pS96 (Figure 5A). GAP-43 was expressed in most of the differentiated neurons, but *in vivo* immunostaining revealed that pS96 was localized only to axonal processes, not to cell bodies (Figures 5 and S4C–S4F), although in culture, the cell bodies were stained by this Ab (Figure 4A). In samples co-stained for the cell adhesion molecule L1 and nuclear DNA (with DAPI), GAP-43 itself was expressed by migrating neurons and ingrowing axons in the intermediate zone (IZ), whereas pS96 was restricted to L1-positive thalamocortical axons in the upper IZ. Such axon-specific expression pattern of pS96 was widely distributed in various fiber tracts of the developing brain (Figure S6):

Adult mice contain continuously renewing olfactory axons, and GAP-43-positive cells represent new neurons derived from stem cells in the basal region of the epithelium (Margolis et al., 1991). We performed immunohistochemistry using the pS96 Ab to determine whether these regenerating, newly growing axons were stained like the growing axons of developing neurons (Figures 5D and 5E). In contrast to the conventional pan GAP-43 Ab, the pS96 Ab more precisely detected growing axons and more heavily immunostained nerve bundles and nerves exiting the olfactory epithelium but did not recognize cell bodies (Figures 5D and 5E).

Taken together, our data show that growing axons *in vivo* were invariably associated with JNK-dependent pS96 of GAP-43, indicating that this Ab represents a new specific molecular marker for growing axons that is superior to anti-pan-GAP-43 Ab.

**pS96 Is a Marker for Axon Regeneration in the Peripheral Nervous System**

Peripheral nervous system (PNS) axons in mammals, including humans, can regenerate (Doron-Mandel et al., 2015). In light of the findings described earlier, we asked whether regenerating PNS axons are

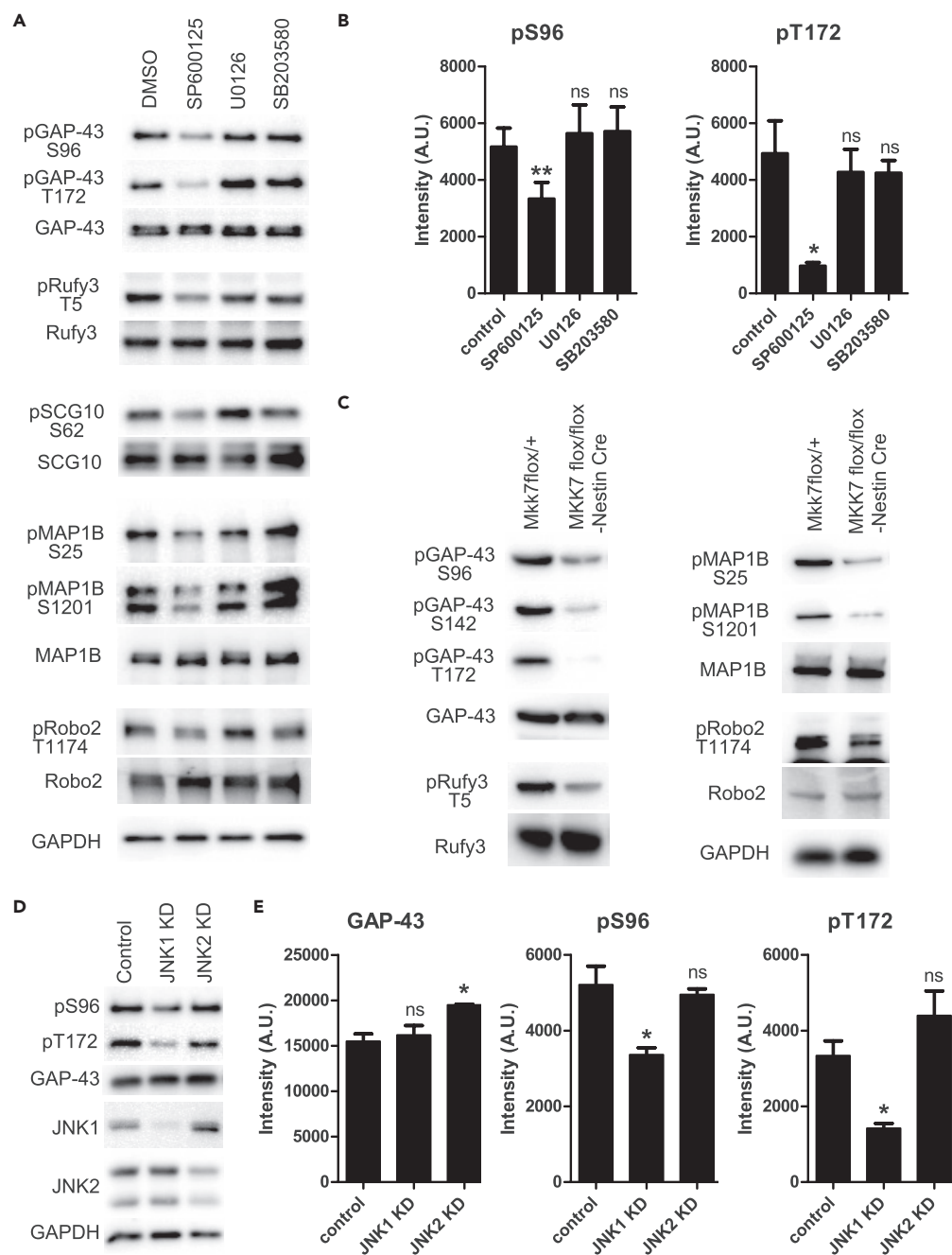


**Figure 3. MAPK Substrates Identified by GCM Phosphoproteomics Undergo JNK-Dependent Phosphorylation**

(A and B) Mouse cortical neurons were treated with 20  $\mu$ M SP600125 (JNK inhibitor), 5  $\mu$ M U0126 (MEK1/2 inhibitor), or 5  $\mu$ M SB203580 (p38 inhibitor) for 3 hr. As a control, an equal volume of the solvent DMSO was added to the medium. (A) The SP/TP phosphorylated sites of various GCM proteins are JNK dependent. Frequencies not appearing in Table S1 are as follows: Robo2 [pT1154] = 25; GAP-43 [pS142] = 18; and Rufy3 [pT5] = 19. Western blot results of non-phosphospecific Abs are shown as negative controls. Kinase inhibitors did not affect the reactivity of any of these non-phosphospecific Abs. (B) Effects of MAPK inhibitors on GAP-43 phosphorylation at S96 and T172. Values represent the measured intensity (mean  $\pm$  SEM, n = 3). \*\*p < 0.01; \*p < 0.05; ns, p > 0.05. One-way repeated measures ANOVA with Bonferroni tests to the control.

(C) Brain-specific cKO of MKK7 (Yamasaki et al., 2011), an upstream activator of JNK, suppressed the identified SP/TP phosphorylation. Brain extracts from WT and MKK7<sup>flox/flox</sup> Nestin-Cre embryos at E15.5 were analyzed by immunoblotting

**Figure 3. Continued**

using the indicated Abs. Western blot results of non-phosphospecific Abs are shown as the controls. Kinase inhibitors did not affect the reactivity of any of these non-phosphospecific Abs.

(D and E) Effects of mouse JNK knock down on GAP-43 pS96 and pT172. The representative western blotting (D) and quantified (E) data. Values represent the measured intensity (mean  $\pm$  SEM, n = 3). \*p < 0.05; ns, p > 0.05. One-way ANOVA with Bonferroni tests to the control. GAPDH: glyceraldehyde-3-phosphate dehydrogenase (A, C, and D).

associated with pS96 of GAP-43. To answer this question, we generated an injury model of the sciatic nerve in mice. In all the mice used for this regeneration analysis, we confirmed the “Sciatic Functional Index for Mouse” (Navarro, 2015) before and after the injury (Savastano et al., 2014). Three days after the nerve crush, we clearly observed pS96 Ab immunoreactivity (Figure 6A), suggesting that the pS96-positive axons elongate with time and that they correspond to regenerating neurons after injury. To quantify the regeneration, we calculated the regeneration index, which is the distance from the injury site to the point where the signal intensity drops by half (Shin et al., 2014). The index for pS96 significantly increased on day 3, consistent with that for SCG10 (Stmn2), another marker of axon regeneration (Figure 6B; Shin et al., 2014). pS96 signals remained low in the intact nerve (Figure 6A). The “crush” vs “intact” ratio of pS96 signal intensity continuously increased until day 7 (Figure 6C), whereas that of GAP-43 transiently increased on day 3 and then decreased on day 7 (Figure 6C), suggesting that pS96 captures axon regeneration more faithfully than GAP-43 itself.

**Detection of pS96 in Regenerating Axons by Phosphoproteomics of Single Injured Sciatic Nerves**

Next, we tried to detect pS96 by MS. For this purpose, samples likely to include regenerating axons were excised from a single sciatic nerve 3 days after injury. After lysis and electrophoresis (Figure 7A), the region of the SDS-PAGE gel corresponding to the position of GAP-43 was cut out and analyzed by liquid chromatography (LC)-MS. This approach positively detected pS96 of GAP-43, and in some cases pS142 (see Figure 3C), another P-directed phosphorylation site of GAP-43 (Figure 7B). These analyses with small samples sensitively and specifically detected pS96 of GAP-43 in regenerating axons, but not in undamaged axons (Figure 7B), consistent with the immunohistochemical results (Figure 6A). By contrast, we could not detect protein kinase C (PKC)-dependent S41 phosphorylation, which had been classically focused on by *in vitro* phosphorylation studies (Skene, 1989; Apel et al., 1990; Denny, 2006) (Figure 7B). Using high-resolution (HR) multiple-reaction monitoring (MRM) for quantification of specific sets of proteins in phosphoproteomics (Figure S7), we confirmed that the level of pS96 GAP-43 was more than 4-fold higher in regenerating axons than in intact nerves (Figure 7C).

These results indicate that pS96 of GAP-43 is tightly associated with PNS axon regeneration and involved in the functional recovery that accompanies regeneration. In addition, these findings confirm that pS96 Ab is a promising molecular marker for regenerating axons, as well as those growing during normal development.

**DISCUSSION**

In this study, we performed quantitative profiling of phosphoproteins and their phosphorylation sites in mammalian GCMs. We obtained three important results: (1) The high frequency of P-directed phosphorylation in GCMs (Figures 2A and 2B; Table S1), as revealed by bioinformatics and biological experiments, was primarily due to MAPKs (Figure 2C), and in particular JNK (Figure 3). (2) The most abundant phosphorylated site, S96 of GAP-43 (Table S1), also underwent JNK-dependent phosphorylation (Figure 3). In addition (3), pS96 was tightly associated with both developmental axon growth (Figures 4, 5, S5, and S6) and axon regeneration (Figures 6 and 7).

Our results suggest that mammalian nerve growth requires activation of JNK. Surprisingly, this conclusion is essentially consistent with the requirement for JNK signaling in axon regeneration, consistent with the results of a large number of mutant screens in *C. elegans* (Hammarlund et al., 2009; Yan et al., 2009; Chen et al., 2011; Andrusiak and Jin, 2016). We conclude that JNK signaling is evolutionarily conserved, even in mammalian axon growth, as demonstrated by the large number of substrates that depend on P-directed kinases. Although S96 phosphorylation was discovered using classical methodology more than a quarter century ago (Spencer et al., 1992), this was before the discovery of JNK (Hibi et al., 1993); however, there have been no reports showing a link between pS96 and JNK to date. We also demonstrated that JNK supports axon growth by modulating vertebrate-specific substrates such as GAP-43 (Figure 3)

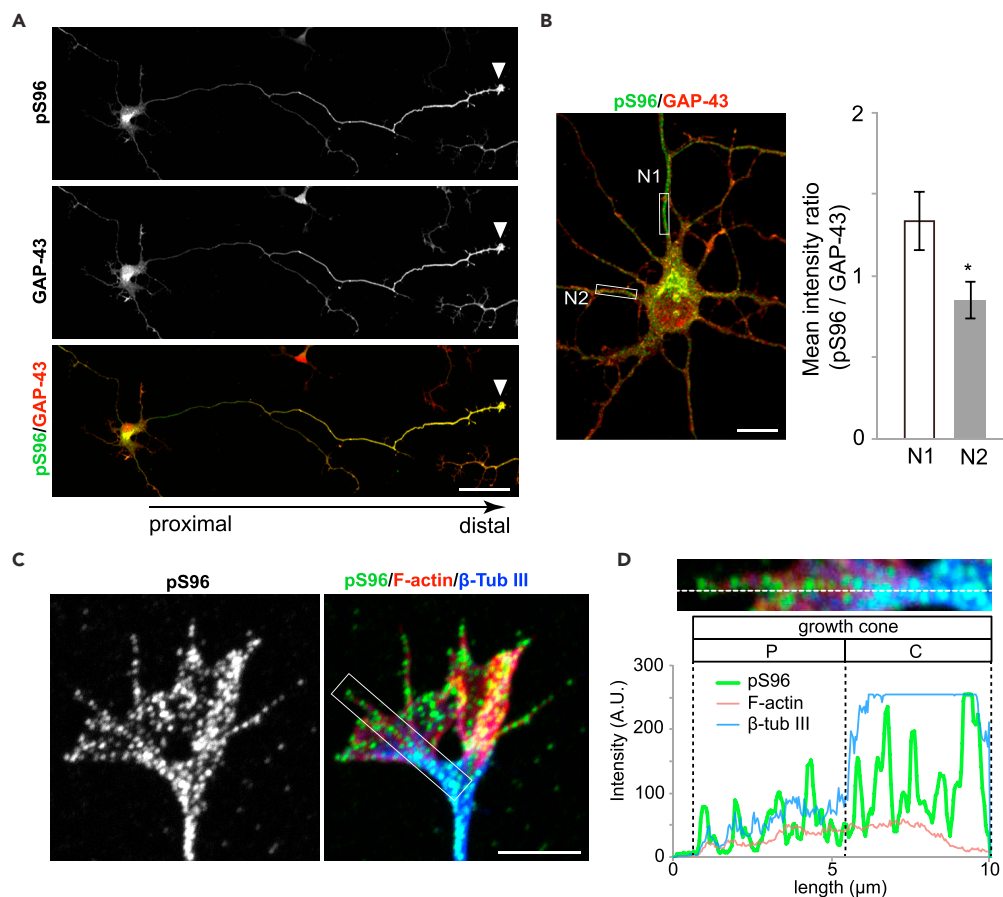


**Figure 4. Antibody Specific for pS96 of GAP-43 Selectively Recognizes Developing and Renewing Axons**

(A and B) Immunostaining of cultured mouse hippocampal neurons (3 days of culture) using antibodies against pS96 (green) and total GAP-43 (red). (A) Full view of a single neuron with a long neurite and a growth cone (arrowhead). Scale bar: 50  $\mu$ m. (B) Magnified view of a soma with several neurites. (Left) White boxes indicate regions of interest (ROI) that were measured. (Right) Means of the staining intensity ratios (pS96 vs pan-GAP-43) in neurites. N1: longest neurite; N2: second-longest neurite. Scale bar: 10  $\mu$ m. Values are expressed as means  $\pm$  SEM; n = 3; \*p < 0.05.

(C and D) Co-localization of pS96 (green) with F-actin (red) and  $\beta$ -tubulin III (blue) in the growth cone of mouse cortical neurons. Scale bar: 5  $\mu$ m. (C) White box indicates the ROI that was measured. (D) Quantitative distribution of the ROI (C) by measuring the fluorescence intensity along the white dashed line from the filopodial tip. P: peripheral domain; C: central domain.

during mammalian development (Holahan, 2017). Although pS96 was found within the supplemental large datasets of the adult mouse brain phosphoproteomics (Huttlin et al., 2010; Lundby et al., 2012), its functions in adult brain is not known.

Our results show that pS96 of GAP-43 is associated with normal mammalian axon growth (Figures 4 and 5) and regeneration (Figures 6 and 7), probably because it is the best substrate for JNK (Table S1). Therefore, the pS96 Ab represents a promising marker for growing and regenerating axons in rodents. Previously, we reported that pS96 Ab could be involved in the regeneration of nerves after surgery (Oyamatsu et al., 2012); however, at that time, the importance of pS96 was not clearly understood. Here, the proteomic results (Figures 2 and 3; Table S1) provide a background against which to understand the importance of this phosphorylation. In addition, pS96 could be detected by MS at high levels, even in a single regenerating segment of injured PNS axons (Figures 7B and 7C). Considering that GAP-43 itself was widely distributed throughout the cell bodies of the developing neurons (Figures 5A–5C) and was present in the intact mature neurons (Figure 6A), pS96 could be used as a strong and specific marker for axon growth and regeneration in rodents. We recently succeeded in performing super-resolution microscopy of the behaviors of live growth cones, revealing new endocytic mechanisms for nerve growth (Nozumi et al., 2017; Nozumi and Igarashi,

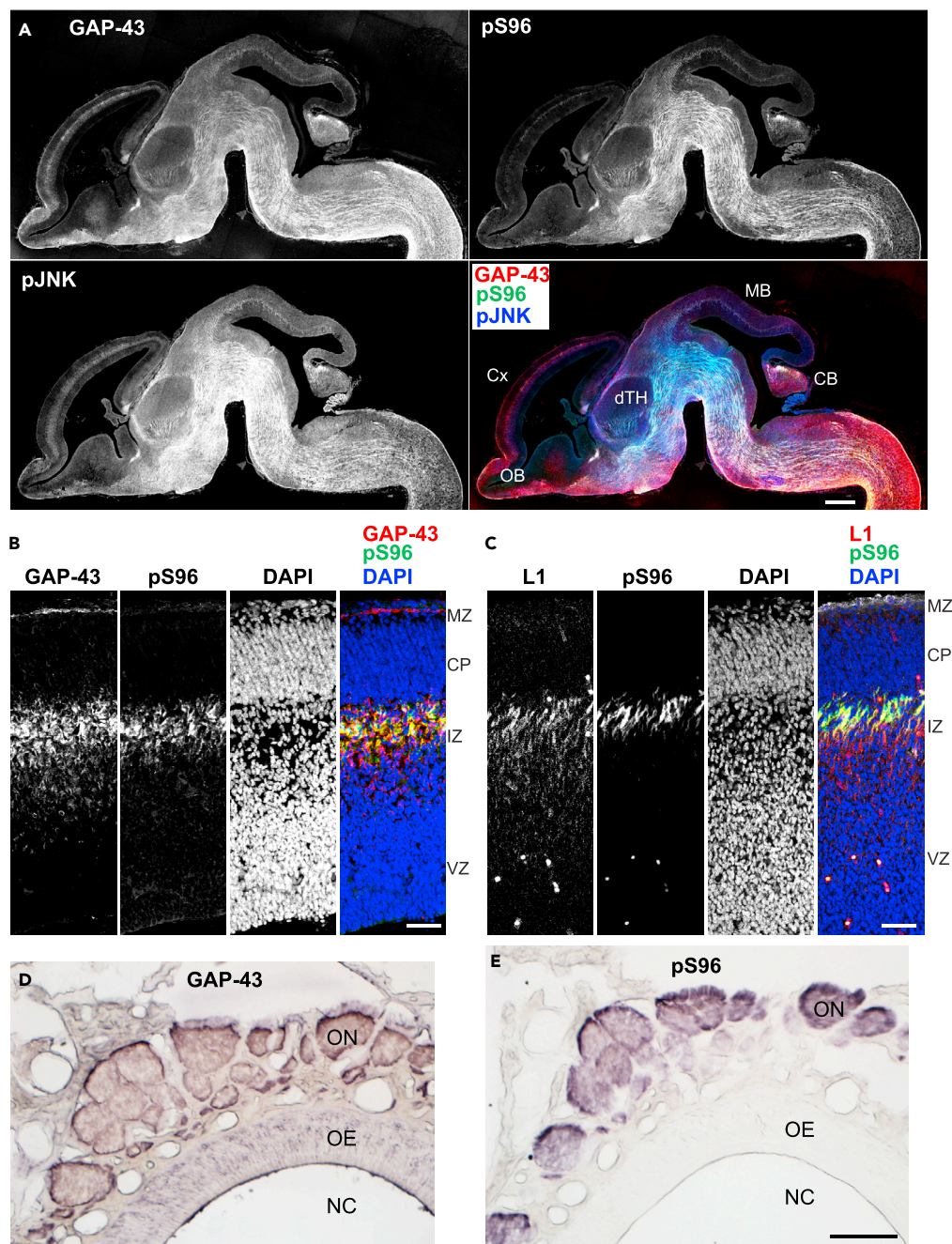


**Figure 5. Expression Pattern of GAP-43, pS96, and pJNK in Developing Mouse Brain**

(A) Expression in an E15 parasagittal section stained with pan-GAP-43, pS96, and pJNK Abs. GAP-43 itself was expressed in most of the differentiated neurons; by contrast, pS96 was localized to axonal processes but was not detected in cell bodies. pJNK exhibited a broader distribution than GAP-43. OB, olfactory bulb; Cx, neocortex; dTH, dorsal thalamus; MB, midbrain; CB, cerebellum.

(B and C) Expression pattern of pS96 and GAP-43 (B) or pS96 and the cell adhesion molecule L1 (C). Nuclear staining with DAPI is also shown. GAP-43 itself was expressed by migrating neurons and ingrowing axons in the intermediate zone (IZ). pS96 expression was restricted to the L1-positive thalamocortical axons in the upper IZ. MZ, marginal zone; CP, cortical plate; VZ, ventricular zone.

(D and E) Expression in the primary olfactory system on P14. GAP-43 itself was expressed in the cells of the olfactory epithelium (OE) and the olfactory nerves (ON; D), whereas pS96 was localized only in the ON (E). NC, nasal cavity. Scale bars: 50  $\mu$ m.

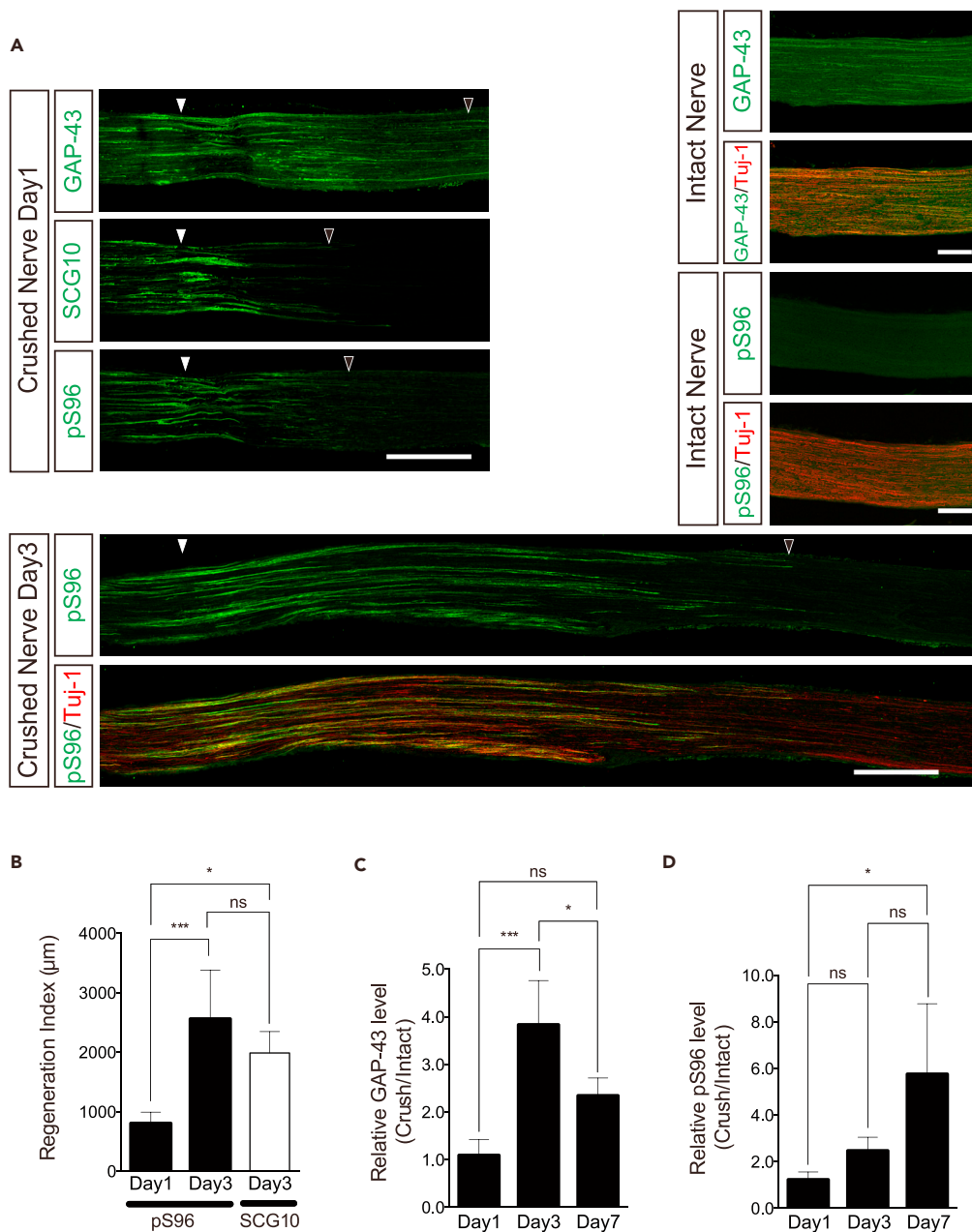


**Figure 6. Axon Regeneration of Injured Sciatic Nerves in Adult Mice Is Strongly Associated with S96 Phosphorylation of GAP-43**

(A) Immunohistochemistry of longitudinal sections of sciatic nerves at days 1 and 3 after crush injury using pS96, total GAP-43, SCG10, and Tuj-1 (neuron-specific  $\beta$ 3 tubulin) Abs. SCG10 was used as a positive control for axon regeneration. Arrowheads (white), injury point; (black), the farthest point of positive immunoreactivity. Intact nerves indicate immunohistochemistry of uninjured nerves. Note that pS96 Ab did not label intact nerves. Scale bars: 500  $\mu$ m (days 1 and 3); 200  $\mu$ m (intact).

(B) Regeneration index (Shin et al., 2014) of pS96 (see Transparent Methods) was higher on day 3 than on day 1. n = 4 (day 1), and n = 6 (day 3); \*p < 0.05, \*\*\*p < 0.001 by one-way ANOVA with Bonferroni tests.

(C and D) Quantification of GAP-43 and pS96 on western blots incubated with their specific Abs. Both crushed sciatic nerves and contralateral, intact ones were excised and subjected to blotting using pan-GAP-43 and pS96 Abs on days 1, 3, and 7 after crushing (n = 4 for days 1, 3, and 7). The blot intensities of the proteins in the intact nerve were used as controls. \*p < 0.05; \*\*\*p < 0.001 by one-way ANOVA with Bonferroni tests. All data in (B–D) are expressed as means  $\pm$  SD.

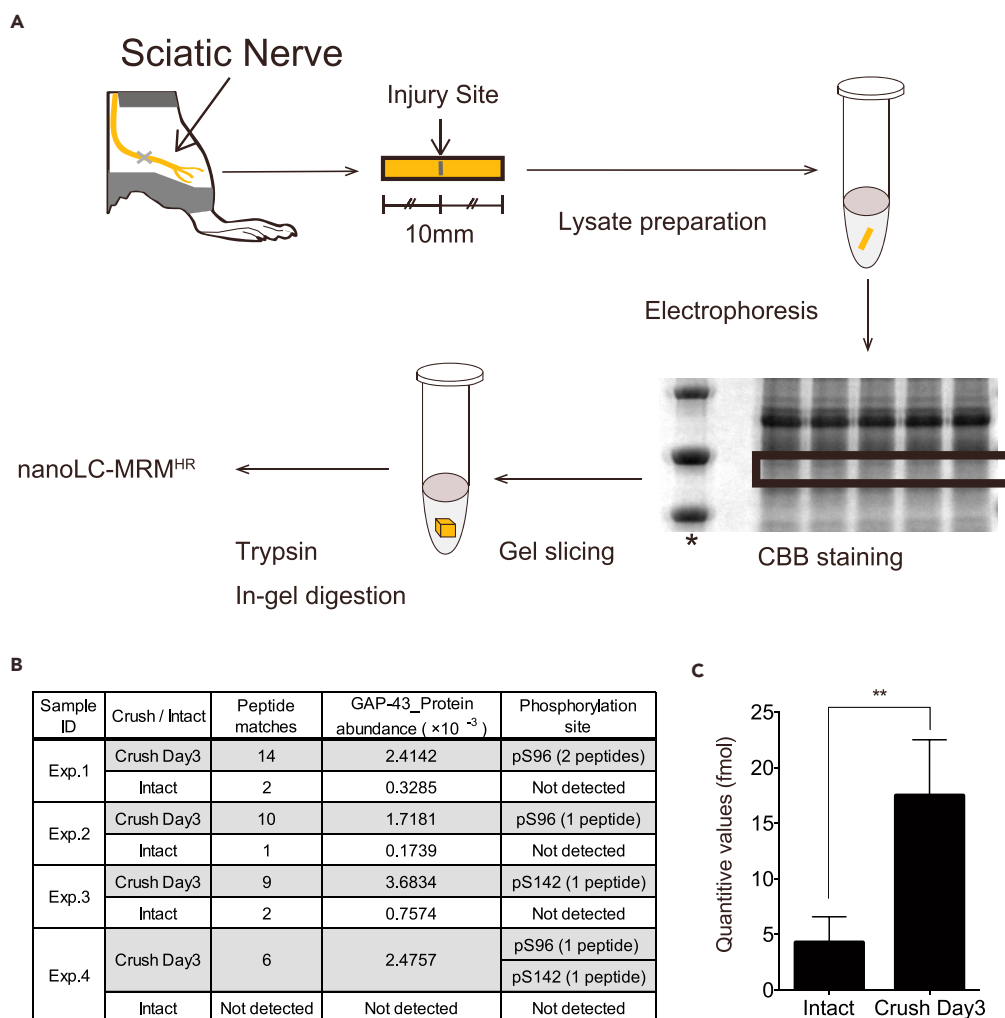


**Figure 7. Phosphoproteomics of a Single, Injured Sciatic Nerve in Adult Mice Reveals that pS96 Is Specifically Detected at Regenerating Axons**

(A) Schematic of phosphoproteomics procedure for a single injured sciatic nerve. The crushed region of a sciatic nerve was excised and divided into 1 cm segments, which were prepared for SDS-PAGE. The band corresponding to GAP-43 was cut out, trypsinized in-gel, and subjected to MS analysis. \*, molecular mass marker.

(B) Shotgun phosphoproteomics analysis of a single crushed nerve. Note that pS96 was detected in three of five injured samples, and another JNK-dependent site, pS142 (Figure 3C), was also detected twice. By contrast, no phosphorylated peptides of GAP-43 were detected in intact nerves.

(C) MS quantification of pS96 using HR-MRM to compare crushed (*Crush*) and intact sciatic nerves on day 3 after injury. *Crush* represents the regenerating axons. \*\* $p < 0.01$  (Student's *t* test). All data are shown as means  $\pm$  SD.

2017). This new method should help reveal the function of pS96 signaling in growth cone behavior much more precisely.

It is important to note that JNK is also a negative regulator of axon growth and can induce axon degeneration (Miller et al., 2009; Tedeschi and Bradke, 2013; Lu et al., 2014; Yang et al., 2015). Accordingly, based on all available data, we conclude that JNK physiologically contributes to axon growth (Yamasaki et al., 2012). The ability to control JNK activity in the near future may lead to effective axon regeneration, enabling clinical treatment of intractable neurological diseases and neural injuries.

## METHODS

All methods can be found in the accompanying [Transparent Methods supplemental file](#).

## SUPPLEMENTAL INFORMATION

Supplemental Information includes Transparent Methods, seven figures, five tables, and three data files and can be found with this article online at <https://doi.org/10.1016/j.isci.2018.05.019>.

## ACKNOWLEDGMENTS

We thank T. Tsubata (ABSciex Co. Ltd.) and M. Matsumoto (Kyushu University, Fukuoka, Japan) for discussions concerning phosphoproteomics, Profs. T. Kanki, M. Komatsu, and H. Takebayashi (Niigata University, Japan) for their comments, and A. Ikarashi (Igarashi laboratory) for excellent technical assistance with the proteomics studies. This work was supported in part by KAKENHI from JSPS and MEXT of Japan (#17023019, #22150003, #22240040, #24111515, #18H04670, and #18H04013 to M.I.; #24110503, #26462232, and #26110703 to K.T.; #23111532, #24650163, #15K14522, and #16H01423 to A.T.; #17K17739 to M.O.; #24700318 and #18K06459 to M.N.; #25870251 to A.K.; #26700029 to S.O.; and #25461212 to Y.Y.); by JST-Presto (to A.T.); and by grants from Yujin Memorial Foundation (to K.T. and M.N.), Kyowa-kai Foundation (to M.O. and D.K.), Takeda Science Foundation (to M.N. and Y.I.), Uehara Memorial Foundation for Life Sciences (to M.I. and Y.I.), and the Project-Promoting Grant from Niigata University (to M.I.). This paper is dedicated as a memorial to the late Karl H. Pfenninger (1944–2015; University of Colorado, Denver, CO, USA), who first established the method for the isolation of growth cones in 1983.

## AUTHOR CONTRIBUTIONS

M.I. conceived the study. A.K. and D.K. performed the biochemical and pharmacological analysis of GAP-43 phosphorylation. M.I., Y.Y., Y.I., and M.O. analyzed the phosphoproteomics of the sciatic nerve. M.I., M.N., T.S., and R.Y. performed the GCM phosphoproteomics. M.I., K.T., and A.K. established and characterized the phospho-specific antibodies. A.T. analyzed immunohistochemistry during development. S.O., A.T., and M.I. performed the bioinformatics analysis. M.I., Y.F., and M.O. designed the nerve regeneration study, and M.O. performed it. H.N. and T.Y. produced and provided the MKK7-cKO mice. M.I. wrote the whole of the manuscript, and M.I., A.K., M.O., A.T., S.O., and Y.Y. wrote the Transparent Methods (see [Supplemental Information](#)) and the legends of the figures.

## DECLARATION OF INTERESTS

R.Y. and T.S. are employees of Sciex Japan. K.T., M.I., M.N., and A.K. have a patent EP2769988 (anti-GAP-43 antibody, date of publication of application: 27 August, 2014), which is related to this work, but there are no patent royalties and licensing fees. Other authors declare no COI.

Received: February 15, 2018

Revised: May 5, 2018

Accepted: May 25, 2018

Published: June 29, 2018

## REFERENCES

- Andrusiak, M.G., and Jin, Y. (2016). Context specificity of stress-activated mitogen-activated protein (MAP) kinase signaling: the story as told by *Caenorhabditis elegans*. *J. Biol. Chem.* *291*, 7796–7804.
- Apel, E.D., Byford, M.F., Au, D., Walsh, K.A., and Storm, D.R. (1990). Identification of the protein kinase C phosphorylation site in neuromodulin. *Biochemistry* *29*, 2330–2335.
- Barnat, M., Enslin, H., Propst, F., Davis, R.J., Soares, S., and Nothias, F. (2010). Distinct roles of c-Jun N-terminal kinase isoforms in neurite initiation and elongation during axonal regeneration. *J. Neurosci.* *30*, 7804–7816.
- Batty, N.J., Fenrich, K.K., and Fouad, K. (2017). The role of cAMP and its downstream targets in neurite growth in the adult nervous system. *Neurosci. Lett.* *652*, 56–63.
- Bloom, O.E., and Morgan, J.R. (2011). Membrane trafficking events underlying axon repair, growth, and regeneration. *Mol. Cell Neurosci.* *48*, 339–348.
- Bogoyevitch, M.A., Ngoei, K.R., Zhao, T.T., Yeap, Y.Y., and Ng, D.C. (2010). c-Jun N-terminal kinase (JNK) signaling: recent advances and challenges. *Biochim. Biophys. Acta* *1804*, 463–475.
- Chang, L., Jones, Y., Ellisman, M.H., Goldstein, L.S., and Karin, M. (2003). JNK1 is required for maintenance of neuronal microtubules and controls phosphorylation of microtubule-associated proteins. *Dev. Cell* *4*, 521–533.
- Chen, L., Wang, Z., Ghosh-Roy, A., Hubert, T., Yan, D., O'Rourke, S., Bowerman, B., Wu, Z., Jin, Y., and Chisholm, A.D. (2011). Axon regeneration pathways identified by systematic genetic screening in *C. elegans*. *Neuron* *71*, 1043–1057.
- Coffey, E.T. (2014). Nuclear and cytosolic JNK signalling in neurons. *Nat. Rev. Neurosci.* *15*, 285–299.
- Denny, J.B. (2006). Molecular mechanisms, biological actions, and neuropharmacology of the growth-associated protein GAP-43. *Curr. Neuropharmacol.* *4*, 293–304.
- Dent, E.W., Gupton, S.L., and Gertler, F.B. (2011). The growth cone cytoskeleton in axon outgrowth and guidance. *Cold Spring Harbor Perspect. Biol.* *3*, <https://doi.org/10.1101/cshperspect.a001800>.
- Doron-Mandel, E., Fainzilber, M., and Terenzio, M. (2015). Growth control mechanisms in neuronal regeneration. *FEBS Lett.* *589*, 1669–1677.
- Ellis, L., Wallis, I., Abreu, E., and Pfenninger, K.H. (1985). Nerve growth cones isolated from fetal rat brain. IV. Preparation of a membrane subfraction

and identification of a membrane glycoprotein expressed on sprouting neurons. *J. Cell Biol.* 101, 1977–1989.

Estrada-Bernal, A., Sanford, S.D., Sosa, L.J., Simon, G.C., Hansen, K.C., and Pfenninger, K.H. (2012). Functional complexity of the axonal growth cone: a proteomic analysis. *PLoS One* 7, e31858.

Gordon-Weeks, P.R., and Fournier, A.E. (2014). Neuronal cytoskeleton in synaptic plasticity and regeneration. *J. Neurochem.* 129, 206–212.

Haeusgen, W., Boehm, R., Zhao, Y., Herdegen, T., and Waetzig, V. (2009). Specific activities of individual c-Jun N-terminal kinases in the brain. *Neuroscience* 161, 951–959.

Hammarlund, M., Nix, P., Hauth, L., Jorgensen, E.M., and Bastiani, M. (2009). Axon regeneration requires a conserved MAP kinase pathway. *Science* 323, 802–806.

Hibi, M., Lin, A., Smeal, T., Minden, A., and Karin, M. (1993). Identification of an oncoprotein- and UV-responsive protein kinase that binds and potentiates the c-Jun activation domain. *Genes Dev.* 7, 2135–2148.

Hirai, S., Banba, Y., Satake, T., and Ohno, S. (2011). Axon formation in neocortical neurons depends on stage-specific regulation of microtubule stability by the dual leucine zipper kinase-c-Jun N-terminal kinase pathway. *J. Neurosci.* 31, 6468–6480.

Holahan, M.R. (2017). A shift from a pivotal to supporting role for the growth-associated protein (GAP-43) in the coordination of axonal structural and functional plasticity. *Front. Cell Neurosci.* 11, 266.

Honda, A., Ito, Y., Takahashi-Niki, K., Matsushita, N., Nozumi, M., Tabata, H., Takeuchi, K., and Igarashi, M. (2017a). Extracellular signals induce glycoprotein M6a clustering of lipid rafts and associated signaling molecules. *J. Neurosci.* 37, 4046–4064.

Honda, A., Usui, H., Sakimura, K., and Igarashi, M. (2017b). Rufy3 is an adapter protein for small GTPases that activates a Rac guanine nucleotide exchange factor to control neuronal polarity. *J. Biol. Chem.* 292, 20936–20946.

Huang, H.D., Lee, T.Y., Tzeng, S.W., and Horng, J.T. (2005). KinasePhos: a web tool for identifying protein kinase-specific phosphorylation sites. *Nucleic Acids Res.* 33 (Web Server issue), W226–W229.

Humphrey, S.J., James, D.E., and Mann, M. (2015a). Protein phosphorylation: a major switch mechanism for metabolic regulation. *Trends Endocrinol. Metab.* 26, 676–687.

Humphrey, S.J., Azimifar, S.B., and Mann, M. (2015b). High-throughput phosphoproteomics reveals in vivo insulin signaling dynamics. *Nat. Biotechnol.* 33, 990–995.

Huttlin, E.L., Jedrychowski, M.P., Elias, J.E., Goswami, T., Rad, R., Beausoleil, S.A., Villén, J., Haas, W., Sowa, M.E., and Gygi, S.P. (2010). A tissue-specific atlas of mouse protein phosphorylation and expression. *Cell* 143, 1174–1189.

Igarashi, M. (2014). Proteomic identification of the molecular basis of mammalian CNS growth cones. *Neurosci. Res.* 88C, 1–15.

Kuan, C.Y., Whitmarsh, A.J., Yang, D.D., Liao, G., Schloemer, A.J., Dong, C., Bao, J., Banasiak, K.J., Haddad, G.G., Flavell, R.A., et al. (2003). A critical role of neural-specific JNK3 for ischemic apoptosis. *Proc. Natl. Acad. Sci. USA* 100, 15184–15189.

Lu, Y., Belin, S., and He, Z. (2014). Signaling regulations of neuronal regenerative ability. *Curr. Opin. Neurobiol.* 27, 135–142.

Lundby, A., Secher, A., Lage, K., Nordsborg, N.B., Dmytriyev, A., Lundby, C., and Olsen, J.V. (2012). Quantitative maps of protein phosphorylation sites across 14 different rat organs and tissues. *Nat. Commun.* 3, 876.

Lundby, A., Andersen, M.N., Steffensen, A.B., Horn, H., Kelstrup, C.D., Francavilla, C., Jensen, L.J., Schmitt, N., Thomsen, M.B., and Olsen, J.V. (2013). In vivo phosphoproteomics analysis reveals the cardiac targets of  $\beta$ -adrenergic receptor signaling. *Sci. Signal.* 6, rs11.

Margolis, F.L., Verhaagen, J., Biffo, S., Huang, F.L., and Grillo, M. (1991). Regulation of gene expression in the olfactory neuroepithelium: a neurogenetic matrix. *Prog. Brain Res.* 89, 97–122.

Miller, B.R., Press, C., Daniels, R.W., Sasaki, Y., Milbrandt, J., and DiAntonio, A. (2009). A dual leucine kinase-dependent axon self-destruction program promotes Wallerian degeneration. *Nat. Neurosci.* 12, 387–389.

Navarro, X. (2015). Functional evaluation of peripheral nerve regeneration and target reinnervation in animal models: a critical overview. *Eur. J. Neurosci.* 30, 1–16.

Nix, P., Hisamoto, N., Matsumoto, K., and Bastiani, M. (2011). Axon regeneration requires coordinate activation of p38 and JNK MAPK pathways. *Proc. Natl. Acad. Sci. USA* 108, 10738–10743.

Nozumi, M., and Igarashi, M. (2017). Vesicular movements in the growth cone. *Neurochem. Int.* <https://doi.org/10.1016/j.neuint.2017.09.011>.

Nozumi, M., Nakatsu, F., Katoh, K., and Igarashi, M. (2017). Coordinated movement of vesicles and actin bundles during nerve growth revealed by superresolution microscopy. *Cell Rep.* 18, 2203–2216.

Nozumi, M., Togano, T., Takahashi-Niki, K., Lu, J., Honda, A., Taoka, M., Shinkawa, T., Koga, H., Takeuchi, K., Isobe, T., and Igarashi, M. (2009). Identification of functional marker proteins in the mammalian growth cone. *Proc. Natl. Acad. Sci. USA* 106, 17211–17216.

Oliva, A.A., Jr., Atkins, C.M., Copenagle, L., and Banker, G.A. (2006). Activated c-Jun N-terminal kinase is required for axon formation. *J. Neurosci.* 26, 9462–9470.

Oyamatsu, H., Koga, D., Igarashi, M., Shibata, M., and Ushiki, T. (2012). Morphological assessment of early axonal regeneration in end-to-side nerve coaptation models. *J. Plast. Surg. Hand Surg.* 46, 299–307.

Savastano, L.E., Laurito, S.R., Fitt, M.R., Rasmussen, J.A., Gonzalez-Polo, V., and Patterson, S.I. (2014). Sciatic nerve injury: a simple and subtle model for investigating many aspects of nervous damage and recovery. *J. Neurosci. Methods* 227, 166–180.

Shin, J.E., Geisler, S., and DiAntonio, A. (2014). Dynamic regulation of SCG10 in regenerating axons after injury. *Exp. Neurol.* 252, 1–11.

Short, C.A., Suarez-Zayas, E.A., and Gomez, T.M. (2016). Cell adhesion and invasion mechanisms that guide developing axons. *Curr. Opin. Neurobiol.* 39, 77–85.

Skene, J.H. (1989). Axonal growth-associated proteins. *Annu. Rev. Neurosci.* 12, 127–156.

Spencer, S.A., Schuh, S.M., Liu, W.S., and Willard, M.B. (1992). GAP-43, a protein associated with axon growth, is phosphorylated at three sites in cultured neurons and rat brain. *J. Biol. Chem.* 267, 9059–9064.

Szklarczyk, D., Morris, J.H., Cook, H., Kuhn, M., Wyder, S., Simonovic, M., Santos, A., Doncheva, N.T., Roth, A., Bork, P., Jensen, L.J., and von Mering, C. (2017). The STRING database in 2017: quality-controlled protein-protein association networks, made broadly accessible. *Nucleic Acids Res.* 45, D362–D368.

Tamada, A., and Igarashi, M. (2017). Revealing chiral cell motility by 3D Riesz transform-differential interference contrast microscopy and computational kinematic analysis. *Nat. Commun.* 8, 2194.

Tedeschi, A., and Bradke, F. (2013). The DLK signalling pathway: a double-edged sword in neural development and regeneration. *EMBO Rep.* 14, 605–614.

Villén, J., Beausoleil, S.A., Gerber, S.A., and Gygi, S.P. (2007). Large-scale phosphorylation analysis of mouse liver. *Proc. Natl. Acad. Sci. USA* 104, 1488–1493.

von Stechow, L., Francavilla, C., and Olsen, J.V. (2015). Recent findings and technological advances in phosphoproteomics for cells and tissues. *Expert Rev. Proteomics* 12, 469–487.

Wong, Y.H., Lee, T.Y., Liang, H.K., Huang, C.M., Yang, Y.H., Chu, C.H., Huang, H.D., Ko, M.T., and Hwang, J.K. (2007). KinasePhos 2.0: a web server for identifying protein kinase-specific phosphorylation sites based on sequences and coupling patterns. *Nucleic Acids Res.* 35, W588–W594.

Yamasaki, T., Kawasaki, H., Arakawa, S., Shimizu, K., Shimizu, S., Reiner, O., Okano, H., Nishina, S., Azuma, N., Penninger, J.M., et al. (2011). Stress-activated protein kinase MKK7 regulates axon elongation in the developing cerebral cortex. *J. Neurosci.* 31, 16872–16883.

Yamasaki, T., Kawasaki, H., and Nishina, H. (2012). Diverse roles of JNK and MKK pathways in the brain. *J. Signal. Transduct.* 2012, 459265.

Yamasaki, T., Deki-Arima, N., Kaneko, A., Miyamura, N., Iwatsuki, M., Matsuoka, M., Fujimori-Tonou, N., Okamoto-Uchida, Y.,



Hirayama, J., Marth, J.D., et al. (2017). Age-dependent motor dysfunction due to neuron-specific disruption of stress-activated protein kinase MKK7. *Sci. Rep.* 7, 7348.

Yan, D., Wu, Z., Chisholm, A.D., and Jin, Y. (2009). The DLK-1 kinase promotes mRNA stability and

local translation in *C. elegans* synapses and axon regeneration. *Cell* 138, 1005–1018.

Yang, J., Wu, Z., Renier, N., Simon, D.J., Uryu, K., Park, D.S., Greer, P.A., Tournier, C., Davis, R.J., and Tessier-Lavigne, M. (2015). Pathological axonal death through a MAPK cascade

that triggers a local energy deficit. *Cell* 160, 161–176.

Zhang, Z., and Cohen, D.M. (1996). NaCl but not urea activates p38 and jun kinase in mIMCD3 murine inner medullary cells. *Am. J. Physiol.* 271, F1234–F1238.

ISCI, Volume 4

## **Supplemental Information**

### **Growth Cone Phosphoproteomics Reveals that GAP-43 Phosphorylated by JNK Is a Marker of Axon Growth and Regeneration**

**Asami Kawasaki, Masayasu Okada, Atsushi Tamada, Shujiro Okuda, Motohiro Nozumi, Yasuyuki Ito, Daiki Kobayashi, Tokiwa Yamasaki, Ryo Yokoyama, Takeshi Shibata, Hiroshi Nishina, Yutaka Yoshida, Yukihiro Fujii, Kosei Takeuchi, and Michihiro Igarashi**

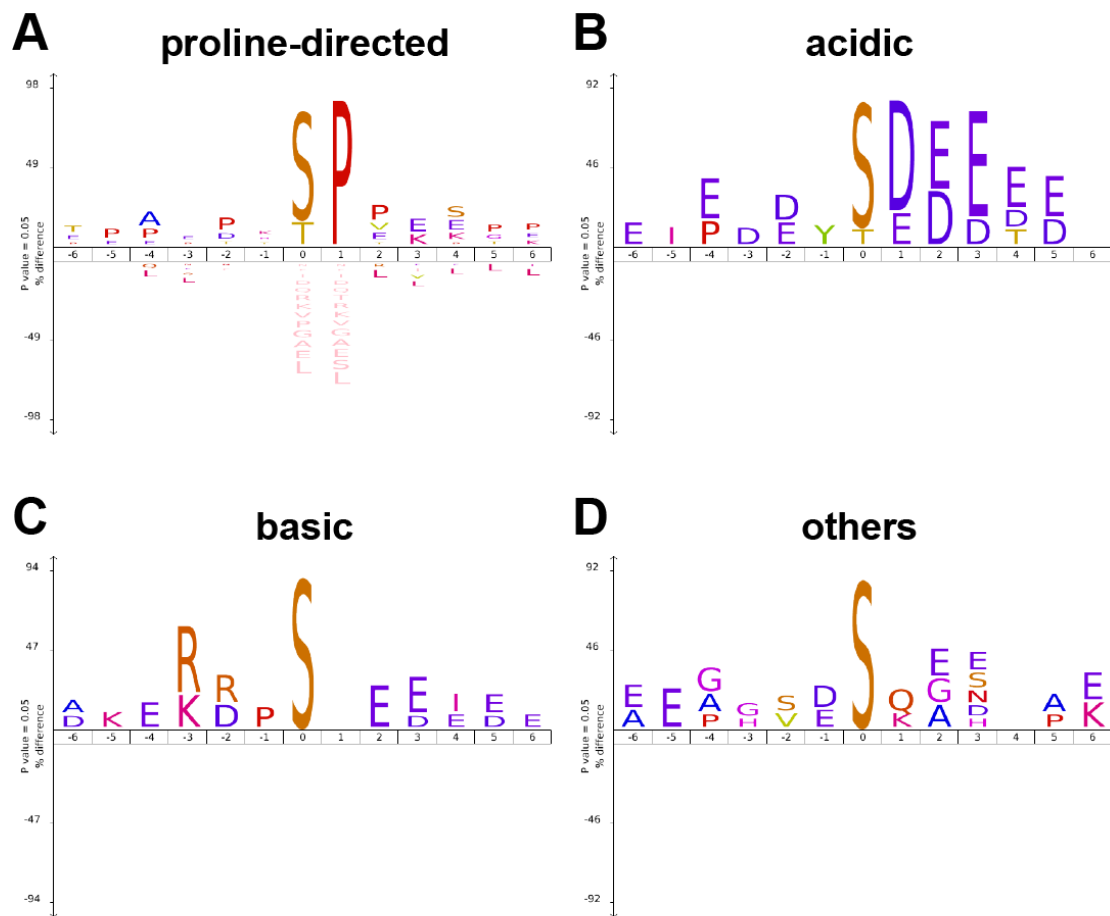


**Figure S1, related to Figure 2. Conserved motif sequence pattern for each phosphosite class, corresponding to the classes of protein kinases (Villén et al., 2007) using the IceLogo web application (Colaert et al., 2009). (A) P-directed, (B) acidic, (C) basic, and (D) other kinases. See also Figure 2A-2B.**

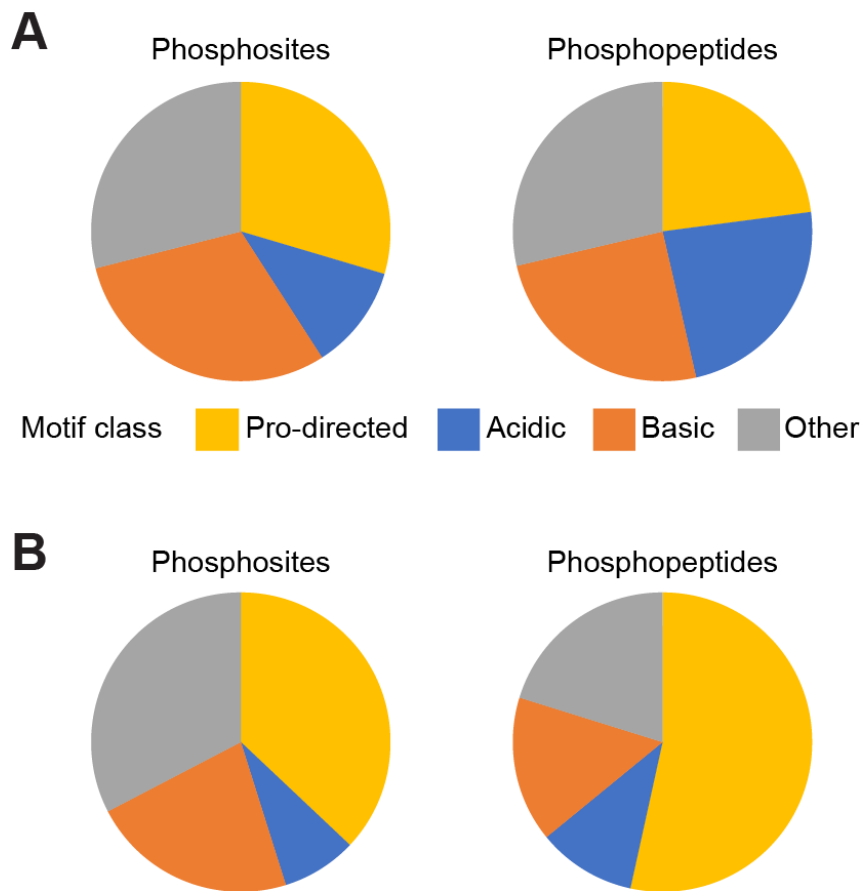


**Figure S2, related to Figure 2. “Meta-analysis” of the data appearing in the phosphoproteomic references (Lundby A et al., 2013 (A); Humphrey et al., 2015b (B)).** Although the data showed a tendency for higher P-directed phosphorylation than that reported by (Huttlin et al., 2010), the percentages of the P-directed sites in our paper were higher than those reported in the two papers above (Figure 2A). Each protein kinase group is defined as Villén et al. (2007). See also Figure 2A.

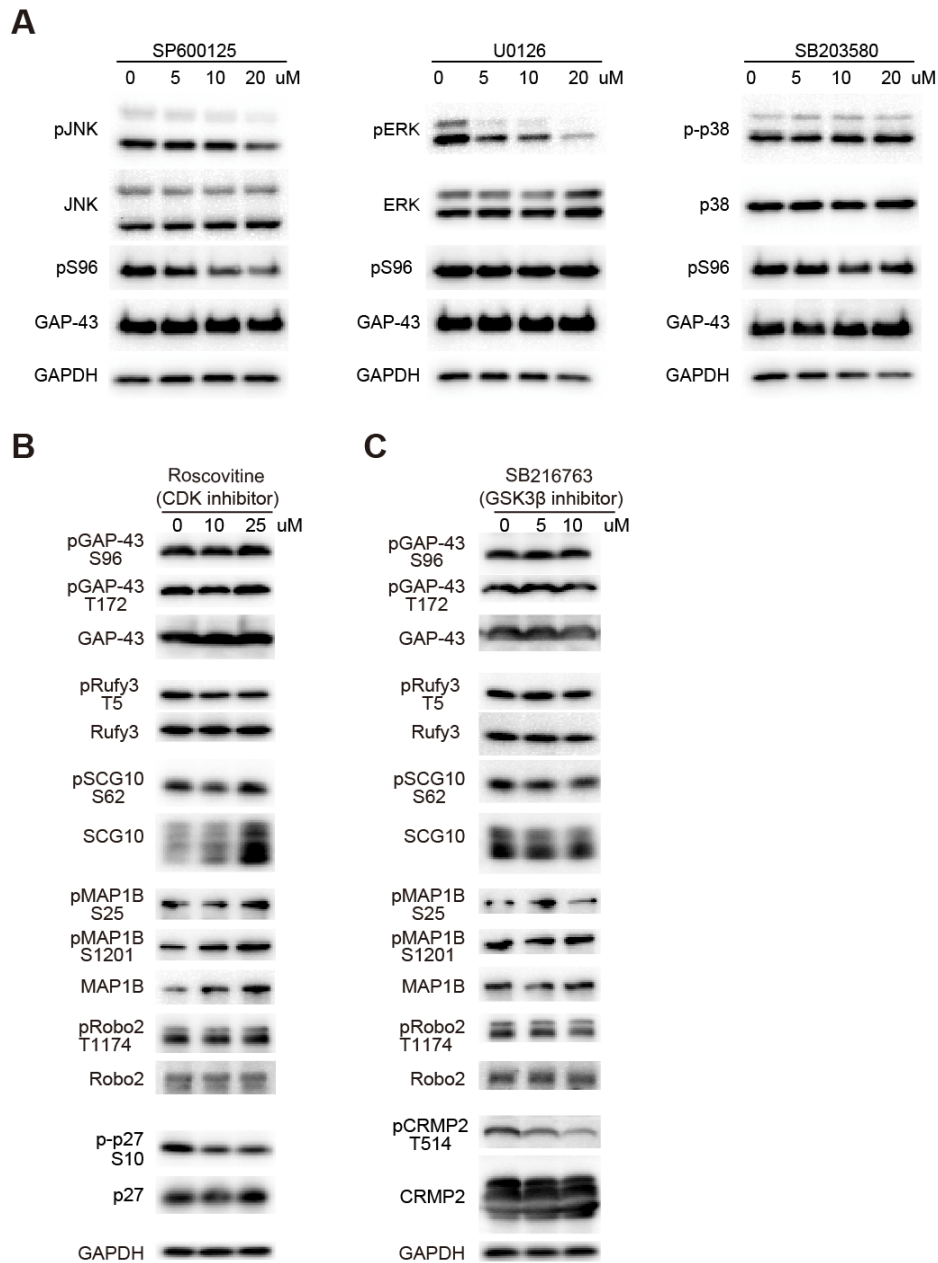


**Figure S3, related to Figure 3. Supplemental results for phosphorylation in cultured mouse neurons in the presence of inhibitors.** (A) Cultured mouse neurons were incubated for 3 h with SP600125, U0126, or SB203580. Each MAPK inhibitor was used at concentrations of 5, 10, or 20  $\mu$ M. SP600125 inhibited the phosphorylation of GAP-43 at S96 in a dose-dependent manner. No significant effect on the phosphorylation of S96 was observed following incubation with U0126 and SB203580. (B, C) CDK (B) and GSK3 $\beta$  (C) were not responsible for the SP/TP phosphorylated sites of the major GCM phosphoproteins. Cultured mouse neurons were treated with roscovitine (a CDK inhibitor; 10 and 25  $\mu$ M) or SB216763 (a GSK3 inhibitor; 5 and 10  $\mu$ M) for 3 h. The inhibitory effect of these inhibitors was evaluated by the phosphorylation levels of p27 (S10) and CRMP2 (T514). As the negative controls, the western blotting results of non-phosphospecific Abs were shown, for all of which the amounts were unchanged in the presence of kinase inhibitors.

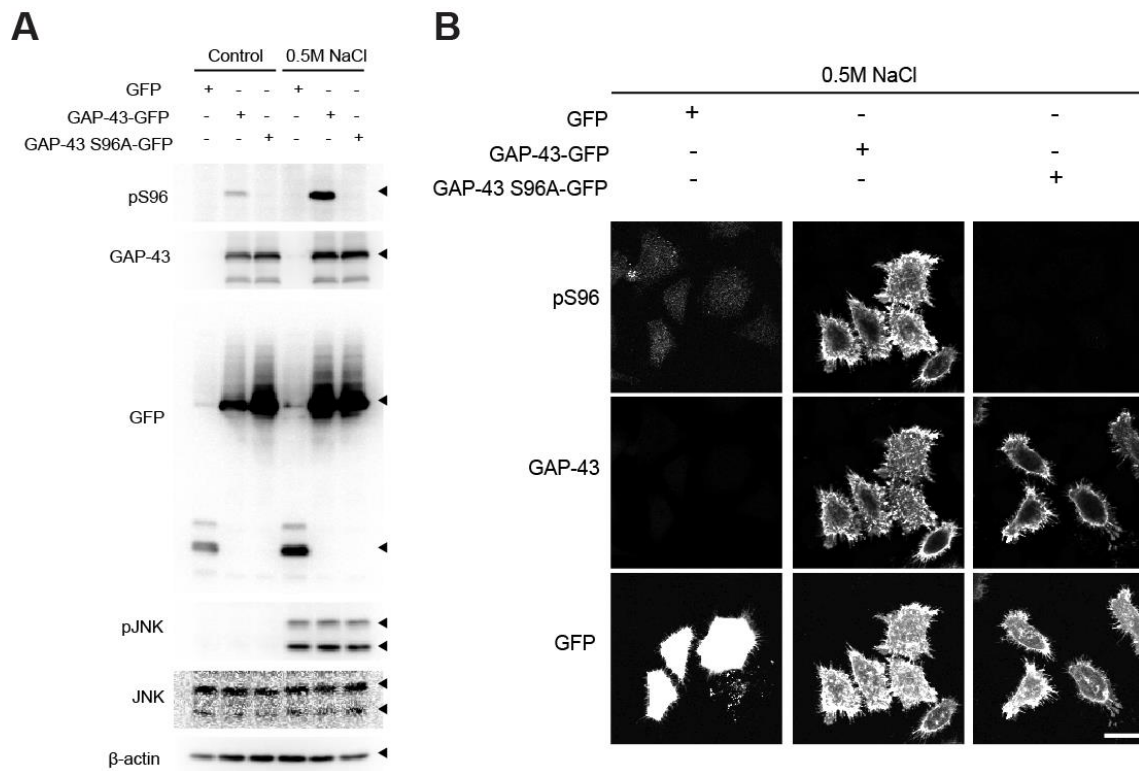


**Figure S4, related to Figure 4. Validation of pS96 Ab specificity in transfected HeLa cells (A, B).** Extracts from the transfected cells were prepared 30 min after osmotic stress (0.5 M NaCl) for JNK activation and immunoblotted using GAP-43, pS96, GFP, pJNK, JNK, and  $\beta$ -actin Abs (A), or the cells were fixed and immunostained with pS96 or pan GAP-43 Abs (B).

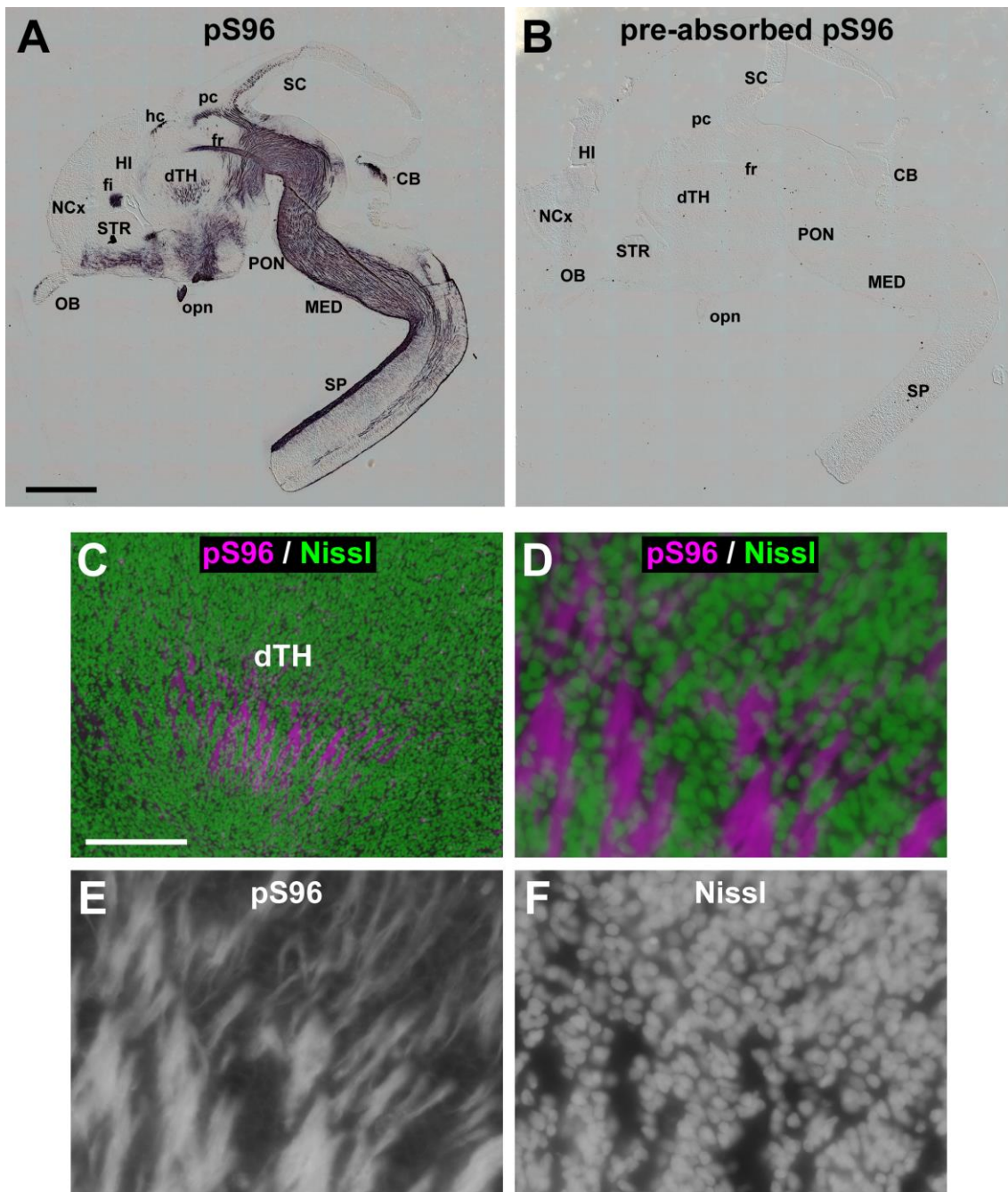


**Figure S5, related to Figure 5. Specificity of the antibody against pS96 and its cellular expression pattern *in vivo*.** (A, B) DIC photomicrographs of adjacent E15 mouse parasagittal brain sections stained with pS96 Ab (A) or pS96 Ab preabsorbed with the immunogen peptide (B) using the Nickel-enhanced DAB method. Scale bar (A):1 mm (A, B). (C) Fluorescent immunostaining of pS96 (magenta) and fluorescent Nissl staining (green) in the dorsal thalamus (dTH) of another section. Scale bar, 200  $\mu$ m. (D-F) High magnification views of (C). Note that pS96 is expressed by thalamocortical axons emerging from the dTH, but is absent in their neuronal somata. The scale bar in (C) represents 50  $\mu$ m (D-F). OB, olfactory bulb; NCx, neocortex; STR, striatum; HI, hippocampus, fi, fimbria; opn, optic nerves; fr, fasciculus retroflexus; hc, habenular commissure; pc, posterior commissure; SC, superior colliculus; CB, cerebellum; PON, pons; MED, medulla; SP, spinal cord.

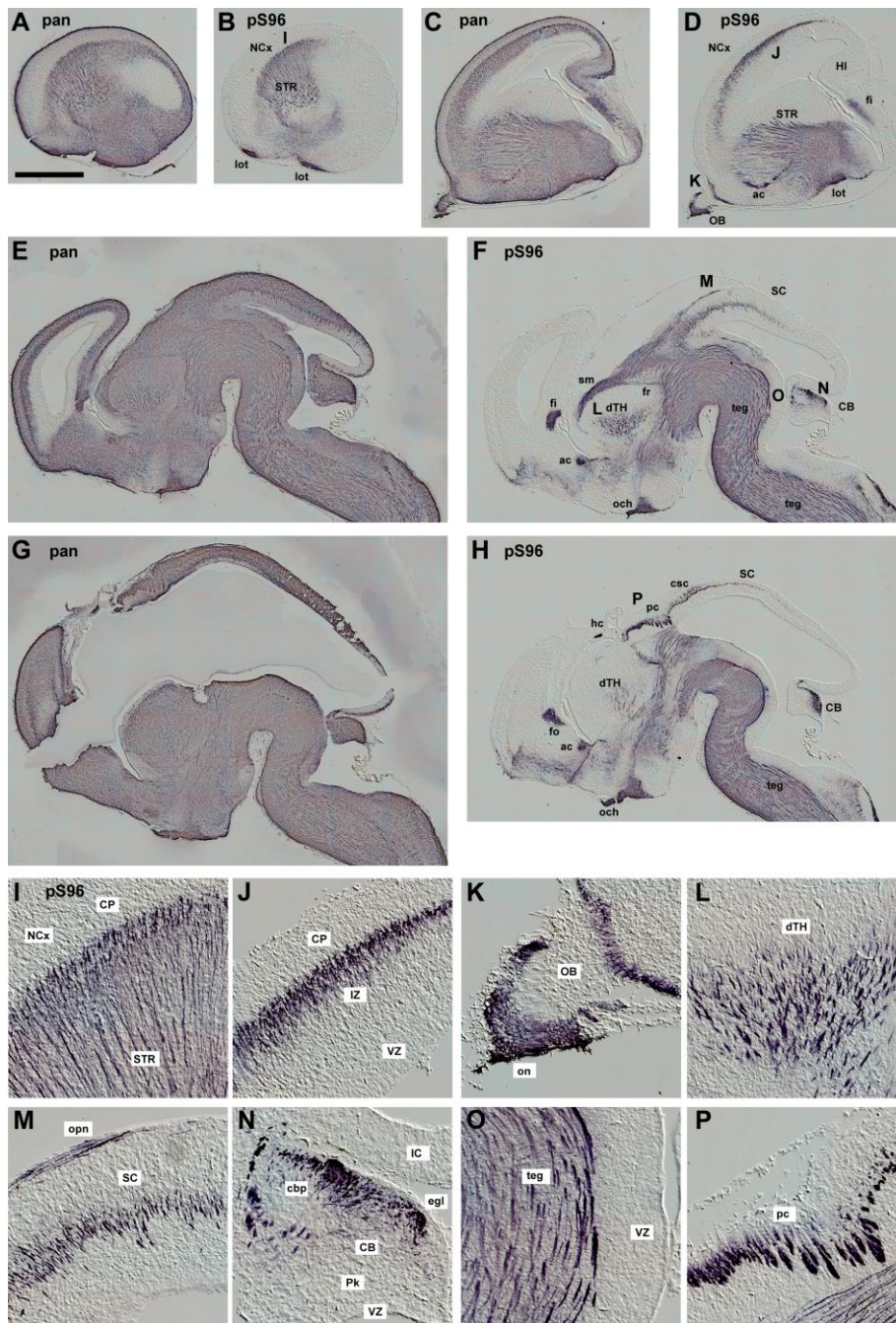


**Figure S6, related to Figure 5. Spatial expression pattern of GAP-43 protein and its pS96 in E15 mouse brain.** (A - H) Photographs of parasagittal sections immunostained with pan-GAP-43 (*pan*; A, C, E, and G) or pS96 Abs (*pS96*; B, D, F, and H). Adjacent sections are displayed in lateral-to-medial order. GAP-43 protein was expressed in most of the differentiated neurons; in contrast, pS96 was confined to the axonal processes and not found in the cell bodies. (I - P) Enlarged views of pS96 staining at the regions marked by letters ((I) in (B), (J) - (K) in (D), (L) - (O) in (F), and (P) in (H)). All pictures are DIC microscopic images of DAB-stained sections. The scale bar shown in (A) represents 1 mm (A - H), or 200  $\mu$ m (I - P), respectively. lot, lateral olfactory tract; ac, anterior commissure; fo, fornix; och, optic chiasm; sm, stria medullaris; teg, longitudinal tegmental tracts; csc, commissure of the superior colliculus; CP, cortical plate; IZ, intermediate zone; VZ, ventricular zone; on, olfactory nerve; IC, inferior colliculus; cbp, cerebellar peduncles; egl, external granular layer; Pk, Purkinje cell layer. See legend of Figure S5 for other abbreviations.

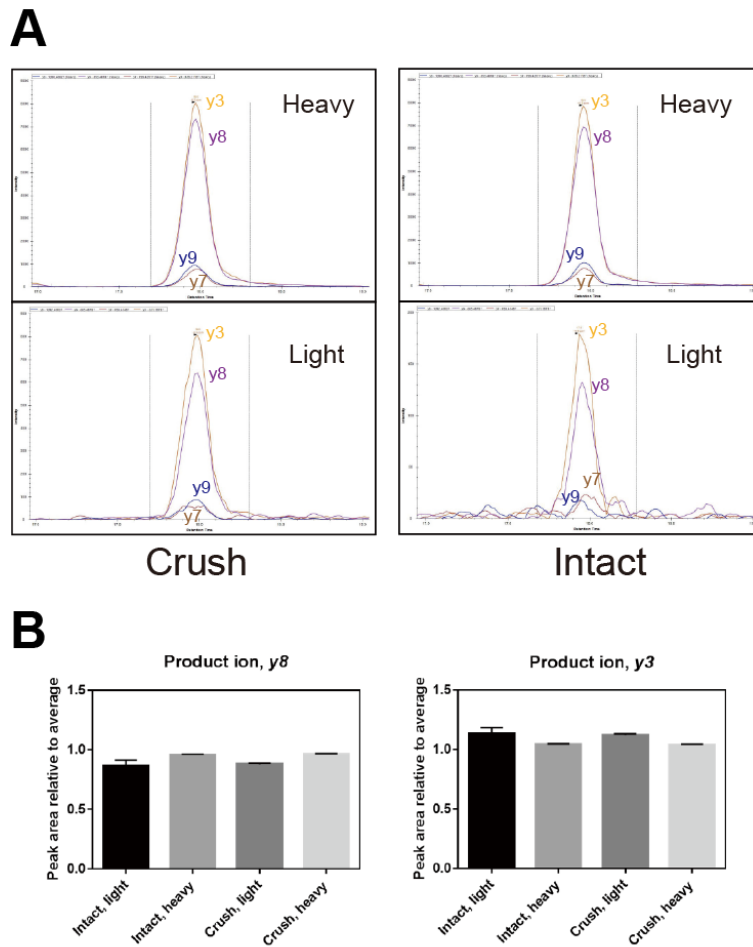


**Figure S7, related to Figure 7. Examination of the peptides used for MRM quantitation of GAP-43 pS96 after sciatic nerve injury in adult mice. (A)** Representative MRM chromatogram of light and heavy target peptides. MRM transitions were built with the aid of Skyline software (see *Methods*) using the peptide sequence (EGDGSATTTDAAPATpSPKAEEPSK). This peptide was phosphorylated at S96 and was found exclusively in the crushed sciatic nerve, according to shotgun proteomic analysis. Note that this peptide contained one missed trypsin cleavage, whereas the pS96-containing peptide without the missed cleavage (EGDGSATTTDAAPATpSPK) was not detected in any samples. We therefore chose the former longer peptide as a target peptide for the MRM assay. **(B)** Quantitation of GAP-43-derived peptides phosphorylated at S96. Note that quantitation was most precise when the transitions producing y8 and y3 ions from the target peptide were selected for MRM. The relative area of the product ion chromatograms was in essentially the same range for the entire set of MRM quantitation assays under the same conditions, indicating no significant interference from other contaminating ions.

**Table S1, related to Figure 1. Major phosphorylation sites with frequencies more than 100 times in GCM derived from rat P1 brain.**

<b>Protein name</b>	<b>Phosphorylation site</b>	<b>Frequency</b>	<b>Kinase group</b>	<b>Protein category</b>
<b>Gap43</b>	S96	542	Proline-Directed	Signaling
Ncam1	S784	503	Basic	Cell Adhesion
<b>Marcksl1</b>	S22	354	Proline-Directed	Signaling
Mtap1b	S1493	350	Proline-Directed	Cytoskeleton
Stmn1	S25	337	Proline-Directed	Cytoskeleton
Stmn2	S62	287	Proline-Directed	Cytoskeleton
Mtap1b	S1304	280	Proline-Directed	Cytoskeleton
Stmn1	S38	265	Proline-Directed	Cytoskeleton
<b>Gap43</b>	T172	245	Proline-Directed	Signaling
Mtap1b	S25	204	Proline-Directed	Cytoskeleton
Mapt	T542	176	Proline-Directed	Cytoskeleton
<b>Marcks</b>	S27	171	Proline-Directed	Signaling
Rras2	S186	162	Proline-Directed	Small GTPase
Mtap1b	S1435	148	Proline-Directed	Cytoskeleton
Ncam1	S888	131	Proline-Directed	Cell Adhesion
Dnajc5	S10	126	Basic	Chaperone
Add1	S12	123	Proline-Directed	Cytoskeleton
Marcks	S46	121	Proline-Directed	Signaling
Map2	T1652	119	Proline-Directed	Cytoskeleton
Mtap1b	S1200	110	Proline-Directed	Cytoskeleton
<b>Marcks</b>	S29	106	Others	Signaling
Mtap1b	S1464	105	Proline-Directed	Cytoskeleton
<b>Dpysl3</b>	S522	100	Proline-Directed	Signaling

The protein name (vertebrate-specific proteins are shown in *bold*), phosphorylation site, phosphopeptide frequency, corresponding protein kinase classification (protein kinase; Villén et al., 2007), and protein classification (see Fig. 1A-1B) are shown.

**Table S2, related to Figure 3. Anti-phospho-specific Abs used in this paper.**

<b>Protein Name (abbreviated)</b>	<b>Accession number</b>	<b>Phosphorylation site</b>	<b>Sequence of antigen peptide</b>	<b>Amino acid number</b>
GAP-43	NM_017195	S96	DAAPATpSPKAE	90-101
GAP-43	NM_017195	T172	VTDAATpTPAAED	165-177
GAP-43	NM_017195	S142	KATTDNpSPSSKA	136-147
Rufy3	NP_001020298	T5	MSALpTPPTDMP	1-11
SCG10	NP_445892	S62	CLILKPPpSPISEA	56-67
MAP1B	NP_062090.1	S25	CNPAATTpSPSLSH	19-30
MAP1B	NP_062090.1	S1201	CASASTIpSPPSSM	1196-1206
Robo2	NP_115289	T1174	CEDRVpTPPVVRG	1167-1179

All antibodies were produced by Sigma-Aldrich. “pS” and “pT” in the column “Antigen Peptide Sequence” indicate phosphoserine and phosphothreonine, respectively.

**Table S3, related to Figure 3. Abs used for immunodetection in this paper.**

Antibody	Supplier	Species	Dilution		
			WB	IF	IHC
$\beta$ -tubulin III (clone TUJ1)	Covance	mouse	-	1:500	-
$\beta$ -tubulin III Biotinylated (clone TUJ1)	R&D systems	mouse	-	-	1:500
GAP-43	Frontier Institute co., ltd	guinea pig	-	1:500	1:2000 - 1:1000
GAP-43	Millipore	rabbit	1:1000	1:1000	-
GAP-43	Sigma	mouse	1:1000	1:200	-
JNK (#9252)	Cell Signaling Technology	rabbit	1:1000	-	-
p-JNK (#4668)	Cell Signaling Technology	rabbit	1:1000	1:500	-
ERK1/2 (#4695)	Cell Signaling Technology	rabbit	1:1000	-	-
p-ERK1/2 (#4370)	Cell Signaling Technology	rabbit	1:1000	-	-
p38 (#8690)	Cell Signaling Technology	rabbit	1:1000	-	-
p-p38 (#4511)	Cell Signaling Technology	rabbit	1:1000	-	-
JNK2 (#9258)	Cell Signaling Technology	rabbit	1:1000	-	-
JNK3 (#2305)	Cell Signaling Technology	rabbit	1:1000	-	-
JNK1 (clone SC-1648)	Santa Cruz Biotechnology	mouse	1:1000	-	-
MAP-1B (sc-8970)	Santa Cruz Biotechnology	goat	1:1000	-	-
Rufy3 (PA5-31311)	Pierce	rabbit	1:1000	-	-
STMN2 (SCG10) (NBP1-49461)	Novus Biologicals	rabbit	1:1000	1:1000	-
Robo2	Tamada et al., 2008	rabbit	1:1000	-	-
GAPDH	MBL Japan	mouse	1:2000 - 1:1000	-	-
p-GAP-43 (S96) (clone 18-10H-9H)	our group / FUJIFILM Wako	mouse	1:1000	1:2000	1:2000
p-GAP-43 (S96)	our group	rabbit	1:1000	1:100	1:1000
p-GAP-43 (T172)	our group	rabbit	1:1000	-	-
p-Rufy (T5)	our group	rabbit	1:1000	-	-
p-Rufy (T51)	our group	rabbit	1:1000	-	-
p-SCG10 (S62)	our group	rabbit	1:1000	-	-
p-MAP1B (S25)	our group	rabbit	1:1000	-	-
p-MAP1B (S1201)	our group	rabbit	1:1000	-	-
CRMP-2 (#35672)	Cell Signaling Technology	rabbit	1:1000	-	-
p-CRMP-2 (T514) (#9397)	Cell Signaling Technology	rabbit	1:1000	-	-
p27	BD	mouse	1:1000	-	-
p-p27 (S10)	Abcam	rabbit	1:1000	-	-
L1 (clone 324)	Merck	rat	-	-	1:500

WB: Western blotting; IF: immunofluorescence; IH: immunohistochemistry.

**Table S4, related to Figure 3. The sequences of siRNAs used in this paper.**

siRNA target	Target sequence (5'→3')
MAPK8 (JNK1)	GGAACGAGUUUUUAUGAUGA
	GUUAGAUCAUGAAAGAAUG
	UCACUCUGCUGGAAUUUAAU
	UUGUUAUCCAAAUGCUAG
MAPK9 (JNK2)	UCACUGUUCUAAAACGUUA
	CUAGCAACAUUGUAGUAAA
	CUGGUAUCAUUCAUAGAGA
	GCCACCACCUCAAUUUUUAAU
control (scramble)	UGGUUUACAUGUCGACUAA

**Table S5, related to Figure 7. Phosphoproteomics of the injured sciatic nerves in adult mice.**

**A**

Animal	Group	Peptide matches	Peptide sequence containing S96	Phosphorylation
#127	Crushed	14	EGDGSATTDAAPATSPK EGDGSATTDAAPATSPK EGDGSATTDAAPAT <b>p</b> SPKAEEPSK EGDGSATTDAAPAT <b>p</b> SPKAEEPSK	S96 S96
#123	Crushed	10	EGDGSATTDAAPATSPK EGDGSATTDAAPATSPK EGDGSATTDAAPAT <b>p</b> SPKAEEPSK	S96
#134	Crushed	9	EGDGSATTDAAPATSPK EGDGSATTDAAPATSPK	
#135	Crushed	4	EGDGSATTDAAPATSPK	
#136	Crushed	6	EGDGSATTDAAPATSPK EGDGSATTDAAPAT <b>p</b> SPKAEEPSK	S96

**B**

Target peptide	Label	Charge	m/z	Product ion
EGDGSATTDAAPATpSPKAEEPSK	Light	3	766.332	y9 y3 y7 y8
EGDGSATTDAAPATpSPKAEEPS[ <sup>13</sup> C(6) <sup>15</sup> N(2)]K	Heavy	3	769.004	y9 y3 y7 y8

(A) The peptides identified containing S96 of GAP-43. The samples from crushed or intact sciatic nerves were separated with SDS-PAGE, and gel slices containing GAP-43 were subjected to in-gel trypsin digestion. Detected phosphorylation of the peptides is shown with italic and bold letters. *Peptide matches*: the number of peptides matched to GAP-43 with a Mascot score larger than the identity threshold and an FDR < 5%. (B) MRM transitions for absolute quantitation of GAP-43 phosphorylated at S96. MRM transitions designed for the absolute quantitation of GAP-43 phosphorylated at S96 were generated using Skyline software version 3.1 (University of Washington). y3 and y8 light product ions were sufficiently intense for accurate quantitation, whereas those of the y7 and y9 ions were too weak to define the peak area, in particular in the intact nerve. We therefore selected the former two ions for the above purpose (see also Figure S7).

## Legends to the Datasets

**Dataset 1. Phosphoproteomics of the GCM proteins.** A: Time; B: Precise molecular weight; C: Precise m/z; D: Precise charge (z); E: Protein number (see Dataset 2); F: Best sequence; G: Modification; H: Confidence; I: Theoretical mass; J: Charge (z).

**Dataset 2. Identified GCM proteins analyzed with phosphoproteomics.** A: Protein number (see Dataset 1); B: Unused; C: Total; D: % coverage; E: Accession number; F: Protein name. *Yellow line*: no phosphorylation-modified peptides were found (only other modifications such as methylation etc.); *Red line*: no phosphopeptides with > 95% reliability were found. They have been deleted from the total counts (Figure 1).

**Dataset 3. Enrichment analysis of the GCM phosphoproteins.** *Category*, KEGG BRITE categories were used for enrichment analysis. The number of enriched genes was counted in the 4th level of the categories. If the number of genes included in a category is lower than four, the category is removed from the calculation. *P-value*, P-value of Fisher's exact test; *Q-value*, FDR adjusted P-value; *Genes*, the genes encoding the identified phosphoproteins in GCM. See also Figure 2D.

## Transparent Methods

**Animals.** All the animal experiments were conducted in compliance with the protocol which was reviewed by the Institutional Animal Care and Use Committee and approved by the President of Niigata University (Permit Number: #26 Niigata Univ. Res.74-2). Postnatal SD rats (Nihon-SLC, Shizuoka, Japan) were used for GCM preparation. Timed-pregnant ICR mice (Nihon-SLC, Shizuoka, Japan) were used for developmental immunohistochemical analysis. Noon of the day on which the plug was detected was designated as E0.5. Brains were removed from the animals that had been deeply anesthetized with sodium pentobarbitone (Nembutal, Abbott, North Chicago, IL, USA; 50 mg/kg of body weight). C57BL/6NCrI mice (Charles River Laboratories Japan, Yokohama, Japan) were used for adult nerve regeneration study (See below).

**Phosphoproteomics analysis of the GCM fraction.** GCM prepared from P1 rat forebrains, its validation, protein extraction, and protein digestions were performed as described previously (Ellis et al., 1985; Gordon-Weeks, 1988; Nozumi et al., 2009). The protein extract (2 mg) from the GCM lysate was suspended in 8 M urea containing 50 mM triethylammonium bicarbonate (TEAB) (pH 8.0). The proteins were reduced by the addition of 50 mM tris(2-carboxyethyl)phosphine and incubated for 2 h at 37°C; the sample was then cooled to room temperature prior to the addition of 20 mM methylmethanethiosulfonate and the cysteines were alkylated for 15 min. The protein mixture was diluted with 50 mM TEAB to a final urea concentration of 1.6 M, then digested by adding 20 µg trypsin (Sciex) and incubating for 16 h at 37°C. The sample was desalted using a Sep-Pak C18 cartridge (Waters Corporation), according to the manufacturer's instructions.

The phosphopeptide mixture was fractionated into six fractions on a strong cation exchange chromatography cartridge (Sciex), using a stepwise gradient of KCl (0, 20, 50, 100, 175, and 350 mM). Each resulting fraction was desalted, solubilized in 0.1% formic acid, and analyzed using a nanoLC-QSTAR Elite mass spectrometer (Sciex) with a NanoSpray III source. Ion source conditions were “ionspray voltage” = 1800 V; “curtain gas” = 20; “declustering potential 1” = 60 V; “focusing potential” = 250 V; and “declustering potential 2” = 15 V. Separation by nanoLC (KYA Technologies) was performed at a constant flow rate of 200 nl/min with a 190-min gradient. A QSTAR Elite mass spectrometer was used in standard MS/MS data-dependent acquisition mode. Survey MS spectra (0.5-sec) were collected (m/z 400-1800), followed by three MS/MS measurements of the most intense parent ions (20 counts/sec threshold, 2-5 charge state, m/z 65-2000 mass range for MS/MS), using the manufacturer's “smart exit” setting 2. Previously targeted parent ions were excluded from repetitive MS/MS acquisition for 60 sec (50 mDa mass tolerance).

All searches were performed against rodent CDS FASTA and annotated with the PANTHER Classification System information. An FDR calculation was performed as described previously (Tang et al., 2008). Phosphopeptide enrichment by IMAC with PHOS Select Iron Affinity Gel (Sigma-Aldrich) was performed essentially as described (Kokubu et al., 2005; Villén and Gygi, 2008). Data files were processed with ProteinPilot 2.0 (Sciex) using the Paragon algorithm (Shilov et al., 2007).

**Bioinformatic analyses of the phosphoproteomic data.** Serine and threonine residues in the phosphopeptides detected by the phosphoproteomics analysis were identified as phosphorylation sites (phosphosites). The counts of the phosphopeptides by the spectroscopy were used as an index that represents the abundance of phosphorylation. Phosphoproteins containing the detected phosphopeptides were classified into 14 functional protein categories. Phosphosites weighted by their counts were similarly classified. The phosphosites were further divided into P-directed and non-P-directed phosphorylation events. Kinases responsible for the identified phosphopeptides were predicted using KinasePhos server (Wong et al., 2007) with 100% specificity. Conserved motif sequence patterns for each phosphosite class were generated with the iceLogo web application (Colaert et al., 2009). The parameters were used as default settings (see Figure S1).

To construct a molecular interaction network (enrichment analysis), KEGG BRITE categories (Kanehisa et al., 2017) were used for enrichment analysis. The number of enriched genes

was counted in the 4th level of the categories. If the number of genes included in a category is lower than four, the category is removed from the calculation. The *STMN2-4* and *DBN1* genes, which are often observed in the category of cytoskeletal modifiers, were not assigned to KEGG Orthology annotations in the version on KEGG BRITE used in this study. Thus, the annotation was manually assigned for these genes prior to performing enrichment analysis. Namely, the protein–protein association data of the STRING database (Szklarczyk et al., 2017) were imported into Cytoscape (Smoot et al., 2011) using the stringApp plugin. See also Figure 2D and Dataset 3.

For “metanalysis” of the high-throughput phosphoproteomics analyses performed by other groups (Lundby et al., 2013; Humphrey et al., 2015b), those phosphoproteomic data were downloaded and re-analyzed. The detected phosphosites were classified into four motif classes, including proline-directed, acidic, basic, and others, according to the following criteria: (1) P at +1 (P), (2) five or more E/D at +1 to +6 (A), (3) R/K at -3 (B), (4) D/E at +1/+2 or +3 (A), (5) two or more R/K at -6 to -1 (B), (6) others (O). The intensities of the phosphosites were added to calculate the fraction. In addition, the intensity value was normalized and the phosphosites with a score  $\geq 20$  or more were extracted for high intensity phosphosites. The fraction of the high intensity groups was calculated as the sum of the original intensity. See Figure S2.

**Western blotting for cells and mouse brains.** The newly generated polyclonal Abs were produced by Sigma-Aldrich, using phosphopeptides as antigens in rabbits (listed in Table S2). The usages of other Abs were summarized in Table S3. Western blotting procedures were described previously (Adachi et al., 2014). The cultured neurons were lysed with TNE buffer (20 mM Tris-HCl [pH 7.5], 150 mM NaCl, 1 mM EDTA, 1 mM phenylmethylsulfonyl fluoride, 1 mM NaF, 1 mM  $\text{Na}_3\text{VO}_4$ , 10  $\mu\text{g}/\text{ml}$  pepstatin, 10  $\mu\text{g}/\text{ml}$  leupeptin, 1% Triton X-100). Experiments using inhibitors of the protein kinases were performed as described previously (Kumar et al., 1999).

**Neuronal culture, RNAi, and pharmacological studies.** Mouse cortical neurons on E15 were dissociated and cultured as described previously (Nozumi et al., 2009). For RNAi experiments, the siRNA sequences (Accell SMARTpool, Dharmacon) used were as follows (Table S4): mouse JNK1 (#E-040128-00) and JNK2 (#E-040134-00). Knock-down efficiency for each siRNA was evaluated by immunoblot analysis 48 h after transfection. Accell Red Non-targeting siRNA (#D-001960-01) was used as a negative control.

**DNA Transfection.** An expression plasmid was constructed for fused protein of rat GAP-43 and EGFP under the control of the CAG promoter. Then, serine-96 was replaced with alanine by KOD-Plus-Mutagenesis Kit (Toyobo). HeLa cells were transfected with these plasmids by polyethyleneimine.

**Immunohistochemistry.** Brains were fixed by immersion in 0.12 M phosphate buffer (PB; pH 7.4) with 4% paraformaldehyde (PFA) for 2-3 days, cryoprotected in 0.1 M PB with 30% sucrose for additional 2-3 days, and embedded in OCT compound (Sakura Finetechnical Co., Ltd., Tokyo, Japan). Coronal sections were cut at a thickness of 20  $\mu\text{m}$  and thaw-mounted on glass slides. Primary Abs used for immunohistochemistry included mouse anti-pS96 (1/2000 dilution) that was biotinylated with Biotin Labeling Kit-NH<sub>2</sub> (Dojindo Laboratories, Kumamoto, Japan), guinea pig anti-pan-GAP-43 (GAP43-GP-Af500, Frontier Institute Co., Ltd., Ishikari, Japan, 1/2000 - 1/1000 dilution) and rat anti-L1 (clone 324, Merck, Darmstadt, Germany, 1/500 dilution). Sections were immunohistochemically stained as previously described (Tamada et al., 2008) with some modifications. All procedures were performed at room temperature. Single immunostaining was performed using a standard avidin–biotin complex (ABC) method (Vectastain ABC Elite kit, Vector Laboratories, Burlingame, CA, USA). Sections were incubated with methanol containing 0.3%  $\text{H}_2\text{O}_2$  for 30 min, washed three times for 10 min each with phosphate buffer saline (PBS) containing 0.2% Triton X-100 (PBST), blocked with 10% normal goat serum (NGS) in PBST for 30 min, and incubated overnight with primary antibodies diluted in NGS-PBST. The next day, sections were washed three times with PBST, reacted with 1/400 biotinylated goat anti-guinea pig IgG (BA7000, Vector) in NGS-PBST for 1 h in the case of pan GAP-43, washed three times with PBST and twice

with PBS, incubated with 1/400 elite ABC in PBS for 1 h, and washed three times with PBS. Color was developed using the nickel-enhanced diaminobenzidine (DAB) method (0.02% DAB, 0.003% H<sub>2</sub>O<sub>2</sub>, 2.5% NiSO<sub>4</sub> in 0.1 M acetate buffer, pH6.0). For multiple fluorescent staining, sections were incubated with the primary antibodies and then with Cy5- or Alexa Fluor 488–conjugated secondary antibodies or Cy3-conjugated streptavidin (all from Jackson ImmunoResearch Inc., West Grove, PA, USA). In some cases, sections were further stained for nuclear DNA with 4', 6-diamidino-2-phenylindole (DAPI; Thermo Fisher Scientific Inc., Waltham, MA, USA) or Nissl-stained with NeuroTrace 500/525 (Molecular Probes, Eugene, OR, USA). DAB-stained samples were observed through an upright microscope (BX63, Olympus, Tokyo, Japan) equipped with differential interference contrast (DIC) optics. Multi-field images were acquired with a CCD camera (DP72, Olympus) and stitched with cellSens software (Olympus). Fluorescence images were acquired with a confocal microscope (FV3000, Olympus) or the upright microscope.

**Immunocytochemistry.** Cultured neurons were fixed with 4% PFA for 15 min at 37°C, permeabilized with PBS containing 0.1% Triton X-100 and 5% BSA for 1hr. Cells were immunostained with the primary and secondary antibodies. For visualization of F-actin, cells were incubated with Rhodamine-phalloidin (Sigma-Aldrich) for 1 h. Fluorescence images were acquired with a confocal laser scanning microscope (FV1200, Olympus).

**Sciatic nerve injury.** Following a standard protocol (Savastano et al., 2014; Shin et al., 2014), male C57BL/6Ncrl mice at 9 weeks of age or older were anesthetized with a cocktail of ketamine and xylazine, and the nerve was crushed with fine forceps (Fontax, INOX #5) for 30 s. The mice were sacrificed on 1, 3, or, 7 days after the operation.

For the immunofluorescence study of the regenerating axons, the mice were perfused intracardially with PBS followed by 4% PFA. Then, the nerves were washed with PBS, immersed in 0.1 M PB with 20% sucrose for an additional 1-2 day, and cut into 20-µm-thick longitudinal sections. The nerve samples were immunostained as described previously (Shin et al., 2012, 2014). Alexa Fluor 488-conjugated Abs or Alexa 594-conjugated streptavidin (Jackson ImmunoResearch Inc.) were used as the secondary Abs. 3D Multiple Fluorescence images were taken with a confocal microscope (FV1200, Olympus) using 10× air objective along the nerve.

Regeneration was evaluated by the regeneration index (Shin et al., 2012; 2014). With ImageJ and MATLAB (Mathworks, USA), 3D stack images were projected along the two axes perpendicular to the nerve and then moving-averaged along the nerve axis to obtain the 1D signal decay. The index was calculated as the distance from the injury site to the point where the signal decays by half.

For western blotting of the sciatic nerves, they were dissected by 1-mm length (see Figure 7A). The samples were homogenized using an ultra-sonicator in sample buffer (125 mM Tris-HCl pH 6.8, 20% glycerol and 4% SDS) with protease inhibitors (10µg/ml leupepsin, 10µg/ml pepstatin, 0.02mM p-APMSF and 1mM EDTA) and phosphatase inhibitors (1.0mM NaF, 1.15mM Na<sub>2</sub>MoO<sub>4</sub> and 1.0mM Na<sub>3</sub>VO<sub>4</sub>). Protein bands were visualized using an ECL Prime kit (GE health care life science, Piscataway, USA). The contralateral intact samples were also used as the control. The relative protein levels recognized by the pan-GAP-43 and pS96 Abs were calculated as the ratio of Crush/Intact nerves.

**MS of regenerating axons.** The protein extract from the injury site or the mock-operated site of the sciatic nerve was prepared as described above. Five equal aliquots of protein extract (19 µg) were separated in parallel on a polyacrylamide gel (ANK KD, Mini-PROTEAN TGX; Bio-Rad Laboratories) and stained with Coomassie Brilliant Blue R-250. The five gel portions containing GAP-43, as indicated by immunoreactivity with anti-pan-GAP-43 Ab, were manually excised and collected in a low-binding microcentrifuge tube for in-gel trypsin digestion. Protein identification was carried out using Mascot version 2.2.1 (Matrix Science).

The gel slices were reduced with 10 mM dithiothreitol, carbamide methylated with 55 mM iodoacetamide, and subjected to in-gel trypsin digestion essentially as described previously (Katayama et al., 2001) to improve recovery of the digested peptides. The peptides from each sample

were finally dissolved in 15  $\mu$ l of 0.2% trifluoroacetic acid and assayed with the BCA method modified for peptide assays (Kappoor et al., 2009). Each sample (5  $\mu$ l, 0.5-0.8  $\mu$ g) was injected into a nano-flow-LC (Eksigent nanoLC 415 with ekspert cHiPLC; Sciex) coupled with a tandem MS (TripleTOF5600; Sciex). Analysis was conducted in duplicate for each sample under trap and elute mode using a ChromeXP C<sub>18</sub> Chip column (200  $\mu$ m  $\times$  0.5 mm) as a trap column, and the same column (75  $\mu$ m  $\times$  150 mm) as the analytical one. Mobile phases A and B were 0.1% formic acid and 0.1% formic acid in acetonitrile, respectively. Peptides were eluted using 30-min gradients from 2% to 32% B at 300 nl/min. MS spectra (250 msec) followed by 10 MS/MS spectra (100 msec each) were acquired in data-dependent mode. The dynamic exclusion time was set at 12 sec. Autocalibration using 50 fmol of tryptic peptides of bovine serum albumin was performed every five to nine samples. Protein identification was carried out using Mascot version 2.2.1 (Matrix Science) as a search engine. The raw data generated by Analyst TF 1.6 (Build 6211) were converted to Mascot generic files by MS Converter (Sciex) and searched against an in-house constructed UniProtKB mouse reference proteome database (49,878 sequences, 29 May 2015 release) using the instrument settings for the ESI-QUAD-TOF spectrometer. The peptide and MS/MS tolerance were set at  $\pm$  20 ppm and  $\pm$  0.1 Da, respectively. Modification settings were: fixed modification, carbamidomethylation of cysteine, variable modifications, deamidation of asparagine and/or glutamine, phosphorylation of serine and/or threonine, N-terminal glutamine to pyroglutamate, N-terminal glutamate to pyroglutamate, and oxidation of methionine. A maximum of two missed cleavages was allowed. The significance threshold was set at  $p < 0.05$ , which gave an FDR of  $< 0.05$  for all identification results. Only peptides with a score exceeding the “Identity threshold” were employed. “Require bold red” was checked to avoid redundancy in protein identification. Quantitation of GAP-43 was performed using the normalized spectral abundance factor (NSAF) (Paoletti et al., 2006). The spectral abundance factor (SAF) was first calculated by dividing the number of spectral counts for each protein by the protein mass or protein length. SAF values were then normalized by dividing by the sum of all SAFs for proteins in a sample to give NSAFs. The schematic procedure is shown in Figure 7A.

**HR-MRM assay for absolute quantitation of pS96 GAP-43 in the crushed nerve.** For HR-MRM, the light (EGDGSATTDAAAPATpSPKAEEPSK;  $m/z = 766.3321$ ) and heavy (EGDGSATTDAAAPATpSPKAEEPS [13C(6)15N(2)]K;  $m/z = 769.0035$ ) peptides were used; the latter was labeled with stable isotopes (SIs; Narumi et al., 2012; Adachi et al., 2016). The internal standard peptide was uniformly labeled with <sup>13</sup>C and <sup>15</sup>N at the carboxyl-terminal lysine (AQUA Peptides, Sigma-Aldrich Life Science). MRM transitions were generated by Skyline software version 3.1 (University of Washington, Seattle, WA, USA). The MRM assay was performed with a TripleTOF 5600+ MS in HR-MRM mode. LC–tandem MS was performed similarly to shotgun analysis.

MRM transitions were built with the aid of Skyline software (University of Washington) using the above light sequence peptide. The peptide contained one missed cleavage by trypsin, while the peptide phosphorylated at S96 without a missed cleavage (EGDGSATTDAAAPATpSPK) were not observed in any samples (Table S5A). Among the 11 peptides matching the corresponding sequence of GAP-43 for five mice, six peptides were shorter and lacked pS96, whereas the other five peptides were longer due to a missed cleavage and contained pS96. None of the shorter peptides contained pS96 (Table S5A). We therefore chose the former longer peptide as a target peptide for the MRM assay.

MRM transitions designed for absolute quantitation of GAP-43 phosphorylated at S96 was generated using Skyline software version 3.1 (Table S5B). Among four transitions selected for light and heavy target peptides, the y3 and y8 product ions of the light peptides were sufficiently strong for accurate quantitation, while those of y7 and y9 ions were too weak to define a peak area, especially in samples from intact nerve (Figure S6A). We therefore selected y3 and y8 ions for calculation of absolute amounts of phosphorylated GAP-43.

To confirm the lack of interference from contaminants in the MRM-HR assay, the peak areas of y3 and y8 relative to their averaged values were compared among all the samples (see Figure 7; Figure S6; Table S5A-S5B). No significant difference between samples was observed,

indicating that there was no significant interference from contaminants in the assay as well as the accuracy of the MRM-HR assay (Figure S6B).

**Statistics.** GraphPad Prism (GraphPad Software) was used for statistical analysis and drawing graphs. Biochemical and culture experiments were analyzed using a Student's *t*-test or one-way *ANOVA* with Bonferroni post-hoc tests. The *p*-value for statistical significance was defined as  $p < 0.05$ . All data are shown as the mean  $\pm$  standard deviation (SD) or mean  $\pm$  standard error of the mean (SEM).

### Supplemental references

- Adachi, J., Narumi, R., and Tomonaga, T. (2016). Targeted phosphoproteome analysis using selected/multiple reaction monitoring (SRM/MRM). *Methods Mol Biol* 1394, 87-100.
- Adachi, M., Kawasaki, A., Nojima, H., Nishida, E., and Tsukita, S. (2014). Involvement of IQGAP family proteins in the regulation of mammalian cell cytokinesis. *Genes Cells* 19, 803-820.
- Colaert, N., Helsens, K., Martens, L., Vandekerckhove, J., and Gevaert, K. (2009). Improved visualization of protein consensus sequences by iceLogo. *Nat Methods* 6, 786-787.
- Gordon-Weeks, P.R. (1988). The ultrastructure of the neuronal growth cone: new insights from subcellular fractionation and rapid freezing studies. *Electron Microsc Rev* 1, 201-219.
- Kanehisa, M., Furumichi, M., Tanabe, M., Sato, Y., and Morishima, K. (2017). KEGG: new perspectives on genomes, pathways, diseases and drugs. *Nucleic Acids Res.* 45: D353-D361.
- Kappoor, K.N., Barry, D.T., Rees, R.C., Dodi, I.A., McArdle, S.E., Creaser, C.S., and Bonner, P.L. (2009). Estimation of peptide concentration by a modified bicinchoninic acid assay. *Anal Biochem* 393, 138-140.
- Katayama, H., Nagasu, T., and Oda, Y. (2001). Improvement of in-gel digestion protocol for peptide mass fingerprinting by matrix-assisted laser desorption/ionization time-of-flight mass spectrometry. *Rapid Commun Mass Spectrom* 15, 1416-1421.
- Kumar S, Jiang MS, Adams JL, Lee JC (1999). Pyridinylimidazole compound SB 203580 inhibits the activity but not the activation of p38 mitogen-activated protein kinase. *Biochem Biophys Res Commun* 263, 825-831.
- Kokubu, M., Ishihama, Y., Sato, T., Nagasu, T., and Oda, Y. (2005). Specificity of immobilized metal affinity-based IMAC/C18 tip enrichment of phosphopeptides for protein phosphorylation analysis. *Anal Chem* 77, 5144-5154.
- Narumi, R., Murakami, T., Kuga, T., Adachi, J., Shiromizu, T., Muraoka, S., Kume, H., Kodera, Y., Matsumoto, M., Nakayama, K., Miyamoto, Y., Ishitobi, M., Inaji, H., Kato, K., and Tomonaga, T. (2012). A strategy for large-scale phosphoproteomics and SRM-based validation of human breast cancer tissue samples. *J Proteome Res* 11, 5311-5322.
- Paoletti, A.C., Parmely, T.J., Tomomori-Sato, C., Sato, S., Zhu, D., Conaway, R.C., Conaway, J.W., Florens, L., and Washburn, M.P. (2006). Quantitative proteomic analysis of distinct mammalian mediator complexes using normalized spectral abundance factors. *Proc Natl Acad Sci USA* 103, 18928-18933.
- Shilov, I.V., Seymour, S.L., Patel, A.A., Loboda, A., Tang, W.H., Keating, S.P., Hunter, C.L., Nuwaysir, L.M., and Schaeffer, D.A. (2007). The Paragon Algorithm, a next generation search engine that uses sequence temperature values and feature probabilities to identify peptides from tandem mass spectra. *Mol Cell Proteomics* 6, 1638-1655.
- Shin, J.E., Cho, Y., Beirowski, B., Milbrandt, J., Cavalli, V., and DiAntonio, A. (2012) Dual leucine zipper kinase is required for retrograde injury signaling and axonal regeneration. *Neuron* 74, 1015-1022.
- Smoot, M.E., Ono, K., Ruscheinski, J., Wang, P.L., and Ideker, T. (2011). Cytoscape 2.8: new features for data integration and network visualization. *Bioinformatics* 27, 431-432.
- Tamada, A., Kumada, T., Zhu, Y., Matsumoto, T., Hatanaka, Y., Muguruma, K., Chen, Z., Tanabe, Y., Torigoe M., Yamauchi, K., Oyama, H., Nishida, K., and Murakami, F. (2008). Crucial roles of Robo proteins in midline crossing of cerebellofugal axons and lack of their up-regulation after midline crossing. *Neural Dev* 3, 29.
- Tang WH, Shilov IV, and Seymour SL. (2008). Nonlinear fitting method for determining local false discovery rates from decoy database searches. *J Proteome Res* 7, 3661-3667.
- Villén J, and Gygi SP. (2008). The SCX/IMAC enrichment approach for global phosphorylation analysis by mass spectrometry. *Nat Protocols* 3, 1630-1638.